PROF. KEVIN T PICKERING (Orcid ID : 0000-0002-7653-1575)

DR. HUGO POUDEROUX (Orcid ID : 0000-0003-4645-0122)

Article type : Original Manuscript

Sedimentology, stratigraphy and architecture of the Nicobar Fan (Bengal–Nicobar Fan System), Indian Ocean: Results from International Ocean Discovery Program Expedition 362

Kevin T. Pickering[1], Hugo Pouderoux[2], Lisa C. McNeill[3], Jan Backman[4], Farid Chemale[5], Steffen Kutterolf[6], Kitty L. Milliken[7], Hideki Mukoyoshi[8], Timothy J. Henstock[3], Duncan E. Stevens[3], Charlie Parnell[3], Brandon Dugan[9]

[1] *Department of Earth Sciences, University College London (UCL), London WC1E 6BT, United Kingdom; kt.pickering@ucl.ac.uk*

[2] *Géosciences, CNRS, Université de Rennes, Rennes 35042, France;*

[3] *Ocean and Earth Science, National Oceanography Centre Southampton, University of Southampton, Southampton S014 3ZH, United Kingdom*

[4] *Department of Geological Sciences, Stockholm University, Stockholm 106 91, Sweden*

[5] *Programa de Pós-Graduação em Geologia, Universidade do Vale do Rio dos Sinos, 93.022-000 São Leopoldo - RS Brasil, Brazil*

[6] *GEOMAR, Helmhotz Center for Ocean Research Kiel, Wischhofstrasse 1-3, Kiel 24148, Germany*

[7] *Jackson School of Geosciences, University of Texas at Austin, 1 University Station, Box X, Austin TX 78713, USA*

[8] *Department of Geoscience, Shimane University, 1060 Nishikawatsu-cho, Matsue-shi, Shimane 690-8504, Japan*

[9] *Department of Geophysics, Colorado School of Mines, Golden CO 80401*

ABSTRACT

Drill sites in the southern Bay of Bengal at 3°N 91°E (International Ocean Discovery Program Expedition 362) have sampled for the first time a complete section of the Nicobar Fan and below to the oceanic crust. This generally overlooked part of the Bengal–Nicobar Fan System may provide new insights into uplift and denudation rates of the Himalayas and Tibetan Plateau. The Nicobar Fan comprises sediment gravity-flow (SGF) deposits, mostly turbidites, that alternate with hemipelagite drapes and pelagite intervals of varying thicknesses. The decimetre-thick to metre-thick oldest pre-fan sediments (limestones/chalks) dated at 69 Ma are overlain by volcanic material and slowly accumulated pelagites (0.5 $g{\cdot}cm^{-2}{\cdot}kyr^{-1}$). At Expedition 362 Site U1480, terrigenous input began in the early Miocene at *ca* 22.5 Ma as muds, overlain by very thin-bedded and thin-bedded muddy turbidites at *ca* 19.5 Ma. From 9.5 Ma, sand content and sediment supply sharply increase (from 1-5 to 10–50 $g{\cdot}cm^{-2}{\cdot}kyr^{-1}$). Despite the abundant normal faulting in the Nicobar Fan compared with the Bengal Fan, it offers a better-preserved and more homogeneous sedimentary record with fewer unconformities. The persistent connection between the two fans ceased at 0.28 Ma when the Nicobar Fan became inactive. The Nicobar Fan is a major sink for Himalaya-derived material. This study presents integrated results of International Ocean Discovery Program Expedition 362 with older Deep Sea Drilling Project / Ocean Drilling Program / International Ocean Discovery Program sites that show that the Bengal–Nicobar Fan System experienced successive large-scale avulsion processes that switched sediment supply between the Bengal Fan (middle Miocene and late Pleistocene) and the Nicobar Fan (late Miocene to early Pleistocene). A quantitative analysis of the submarine channels of the Nicobar Fan is also presented, including their stratigraphic frequency, showing that channel size/area and

abundance peaked at *ca* 2 to 3 Ma, but with a distinct low at 3 to 7 Ma: the intervening stratigraphic [sub]unit was a time of reduced sediment accumulation rates.

Keywords: Bengal Fan, Indian Ocean, IODP Expedition 362, Nicobar Fan, sediment gravity flow, submarine fan, Sunda Subduction Zone

INTRODUCTION

The Bengal-Nicobar Fan System (BNFS) is one the largest and oldest active deep-marine sedimentary systems on Earth. The confluence of the Ganges and the Brahmaputra rivers in the Bengal Delta drain the eastern and central Himalaya Range and Tibetan Plateau (1.59 x 10^6 km^2) to deliver enormous amounts of material into the northern Indian Ocean (*ca* 1060 x 10^6t yr^{-1}; Milliman & Syvitski, 1992). The western Himalaya Range and Tibetan Plateau are drained by the Indus River (0.97 x 10^6 km^2), which supplies the Indus Fan in the Arabian Sea (*ca* 250 x 10^6t yr^{-1} before dam constructions; Milliman & Syvitski, 1992; Clift *et al.*, 2001; Clift, 2002). Together, the BNFS and Indus Fan preserve important sedimentary archives of the formation and denudation history of the Himalaya Range since the India–Asia collision onset in the Palaeocene–Eocene.

The BNFS extends over an area of *ca* 4 x 10^6 km^2 in the northern Indian Ocean to encompass the Bengal Delta, the Bangladesh continental shelf and a large submarine fan system (i.e. the Bengal–Nicobar fans) that covers the entire floor of the Bay of Bengal, reaching as far south as Sri Lanka and south of Sumatra at its western and eastern extents, respectively (Fig. 1). Huge volumes of sediment are created by the continuous denudation of the central and eastern Himalaya Range to accumulate in the BNFS (>8 x 10^6 km^3 since *ca* 20 Ma; Curray & Moore, 1971; 1974; Curray *et al.*, 2014; McNeill *et al.*, 2017a).

The BNFS has been studied for the last 50 years to investigate the structure and development of large submarine fans, and the links between India–Asia tectonics, Himalayan denudation and Asian monsoons (Curray & Moore, 1971; Emmel & Curray, 1984; France-Lanord *et al.*, 1993; Curray *et al.*, 2003; Schwenk & Spiess, 2009). However, apart from IODP Expedition 362 and one drill site on DSDP Leg 22 Site 211, the rest of the DSDP, ODP and IODP expeditions in the region have targeted the Bengal Fan, which covers five sixths of the surface area of the deep-sea part of the modern BNFS. The Nicobar Fan, which develops in

the eastern side of the system, is largely undersampled even though it contains key information on the tectonostratigraphic evolution of the eastern Indian Ocean (McNeill *et al.*, 2017a). DSDP Site 211 (von der Borch, Schlater *et al*., 1974) contains a tongue of siliciclastic sediments south of Sumatra and isolated from the Nicobar Fan and, because of its proximity to the Investigator Fracture Zone, has been designated as the 'Investigator Fan' (Fig. 1). It is most likely an isolated part of the distal Nicobar Fan (fan lateral margin) that has yet to be incorporated into the Sunda subduction zone accretionary prism.

International Ocean Discovery Program (IODP) Expedition 362 (August to October 2016) sampled and logged a complete section of the Nicobar Fan seaward of the subduction zone of North Sumatra down to the oceanic crust (Dugan *et al.*, 2017; McNeill *et al.*, 2017a; b). Designed to investigate the causes of shallow seismogenesis, tsunamigenesis and forearc development of the Sunda subduction zone system where the 2004 M_w 9.2 earthquake struck, IODP expedition 362 also offers a unique opportunity to precisely determine the lithologies, properties and sedimentation rates of the material emplaced in the Nicobar Fan since its formation.

This paper presents the main results of IODP Expedition 362 in terms of sedimentology, architecture and stratigraphy of the Nicobar Fan. Coupled with re-interpreted regional seismic data, these permit discussion of the depositional history of the Nicobar Fan and its relationship with the Bengal Fan. Therefore this study can propose more comprehensive palaeogeographic reconstructions of the entire BNFS since the early Oligocene.

SETTING

Bengal depositional fan

The formation of the Bengal Fan results from the northward movement and collision of India into southern Asia with sediment supply driven by uplift and denudation processes (Curray, 2014). Since its discovery in the 1950s/1960s, the Bengal Fan has been studied to characterize its shape, extent and controlling parameters (Curray & Moore, 1971; Curray *et al.*, 2003; France-Lanord *et al*., 2016), which were then used as a geological archive of past climatic fluctuations, tectonic activity and oceanographic conditions of the northern Indian Ocean region (Schwenk & Spiess, 2009; Joussain *et al.*, 2016). Sediment volumes preserved

in the BNFS record the denudation history of the Himalaya Range and have been used to estimate denudation rates over geological timescales (France-Lanord *et al.*, 1993; Einsele *et al.*, 1996; Métivier *et al.*, 1999), whereas variations in the nature and rate of sediment accumulation were related to regional climatic variations (France-Lanord *et al.*, 1994; Weber *et al.*, 2003). Recently, studies have shown the importance of the Bengal Fan in the carbon cycle via uplift and denudation processes in the India–Asia collision zone (carbon dioxide consumption from silicate weathering) and marine sedimentation (burial of organic carbon), which makes the Bengal Fan a net sink of CO_2 at a global scale (France-Lanord and Derry, 1997; Galy *et al.*, 2007; Lee et al, 2019).

The Bengal Fan has commonly been used as a natural laboratory to understand deep-marine sedimentation and sediment gravity-flow (SGF) processes and dynamics (e.g. Reading & Richards, 1994; Covault & Graham, 2010) and as a well-documented analogue for submarine-fan reservoirs (Fergusson & Coney, 1992), and potential oil and gas prospects (Bastia *et al.*, 2010; Yang and Kim, 2014).

Nicobar Fan

East of the Bengal Fan and separated from it by the Ninetyeast Ridge, the Nicobar Fan and associated Sunda Subduction Zone are important but often overlooked parts of the BNFS, until IODP Expedition 362. Thick sedimentary successions are found within Nicobar Fan and accreted at the Sunda subduction zone (for example, Oligocene Andaman Flysch), suggesting that these components have served as significant depocentres for Himalayan-derived source material in the BNFS since its initiation in the Palaeocene–Eocene (Fig. 1). For example, the *ca* 3000 m thick Oligocene so-called 'Andaman Flysch' in the northern part of the Sunda Subduction Zone is interpreted as accreted Himalaya-derived BNFS deposits (Curray *et al.*, 1979), with lesser contributions from other sedimentary and volcanic material, possibly the Shan-Thai continental block and volcanic arc in Myanmar (Bandopadhyay & Ghosh, 2015).

The Nicobar Fan is a *ca* 0.5 x 10^6 km^2 deep-marine depositional system located in the northern Indian Ocean, south-east of the *ca* 3 x 10^6 km^2 Bengal Fan. It extends from 7°N to 9°S and from 90° to 95°E and is located in a *ca* 0.65 x 10^6 km^2 wide depression flanked by the Ninetyeast Ridge to the west and the Sunda Subduction Zone to the east (Fig. 1). In contrast to the rich Holocene record preserved in the SGF deposits of the Bengal Fan, the

Nicobar Fan is mostly inactive today (i.e. abandoned) because of impingement of the Ninetyeast Ridge with the subduction zone at the latitude of the Andaman Islands (*ca* 10°N) in the late Pleistocene, which blocked sediment supply from the north (Curray & Moore, 1974; Moore, 1982).

Little information exists for the timing, architecture and depositional history of the Nicobar Fan prior to IODP Expedition 362. Deep Sea Drilling Project (DSDP) Site 211 in the southern edge of the fan at 9°S is the only available dataset that penetrated the fan (von der Borch *et al.*, 1974; Fig. 1), but this site was only spot cored. Drilling results showed a *ca* 250 m thick unit composed of mica-rich quartzo-feldspathic sand and silt beds deposited from SGFs buried beneath a *ca* 100 m thick pelagite section. These are likely fan lateral-margin deposits from a now accreted distal part of the Nicobar Fan. The SGF deposits at DSDP Site 211 are poorly dated but the last occurrence and, therefore, the age of this abandoned segment of the Nicobar Fan at this location (*ca* 9°S), is assumed to be late Miocene [Appendix Fig. 1; Appendix Table 1; after von der Borch *et al.* (1974)]. From the Pliocene onward, terrigenous sediment supply to DSDP Site 211 ceased, potentially due to collision and accretion into the Sunda subduction front (Fig. 1).

International Ocean Discovery Program Expedition 362

Sites U1480 and U1481 are located at 3°N 91°E, *ca* 250 km west of the Sunda Subduction Zone, on the eastern flank of the Ninetyeast Ridge where the input section to the subduction zone is *ca* 1.5 km thick (Fig. 1). They were drilled, cored and logged to a maximum depth of 1500 m below seafloor (mbsf), and reached the 60 to 70 Ma igneous oceanic crust of the Indian plate (Dugan *et al.*, 2017; McNeill *et al.*, 2017a; b). The two sites are *ca* 35 km apart making them at the same proximity to the source of the fan (Fig. 1). The recovered sediments represent a latest Cretaceous to late Palaeocene interval and a nearly continuous early Miocene through Recent interval, separated by a *ca* 41 Myr long hiatus (McNeill *et al.*, 2017b; Backman *et al.*, 2019). The Miocene–Quaternary interval consists of siliciclastic sediments deposited from various SGFs (including turbidity currents and debris flows), interpreted as Nicobar Fan deposits, underlain by abyssal-plain environment sediments containing hemipelagic, pelagic, tuffaceous and igneous lithologies overlying ocean crust (Fig. 2; McNeill *et al.*, 2017a; b).

Six lithological units were identified by IODP Expedition 362 (LU-I to LU-VI from top to base; Figs 2 and 3), some of which are divided into lithological subunits based on the vertical organization of the dominant lithologies (Dugan *et al.*, 2017). Lithological units and subunits I, IIA to IIC and IIIA contain siliciclastic sediments of the Nicobar Fan to a depth of 1250.35 mbsf (Site U1480). The oldest fan sediments occur in LU-IIIA (1250.35 to 1310.10 mbsf and are early Oligocene to late Miocene). They occur as mainly thin to medium-bedded, grey-green or brown mudstone of very clay rich composition (claystones) and intercalated siltstones. Beds have diffuse parallel lamination towards their base and scattered agglutinated foraminifera in structureless mudstone caps. Throughout the cores, there are rare and isolated, very thin-bedded siltstones, characteristically showing parallel lamination. Some beds grade from silty claystone at the base to claystone tops with increasing upward bioturbation. Core disturbance is commonly observed (see Appendix Table 2 for types of drilling disturbance).

Directly below the seafloor, LU-I (0 to 26 mbsf) consists of biogenic calcareous muds with ash beds (LU-IA and LU-IC) and siliciclastic fine-grained sands and muds (LU-IC). Subunit LU-II (26 to 1250 mbsf) is mostly composed of alternating beds of quartzo-feldspathic siliciclastic sands and muds enriched in micas and plant debris (LU-IIA to LU-IIC) with rare ash and biogenic calcareous mud beds. Subunit LU-III (1250 to 1327 mbsf) is composed of stacked grey-green siliciclastic mudstone beds (LU-IIIA) overlying reddish-brown tuffaceous mudstones with rare chalk beds (LU-IIIB). Subunit LU-IV (1327 to 1350 mbsf) is composed of basaltic flows and volcanic material, and LU-V (1350 to 1415 mbsf) is marked by stacked magmatic intrusions within calcareous mudstones and chalks. Finally, LU-VI (1415 to 1432 mbsf) is entirely made up of basalts.

Subunits LU-IIIB to LU-V are interpreted as pre-fan deposits while LU-VI is identified as the basaltic crust of the Indian Plate (Dugan *et al.*, 2017; McNeill *et al.*, 2017b). The basal part of the Nicobar Fan (LU-IIIA), unlike LU-IIC with thin sandstone beds, only contains siliciclastic mudstones and is here interpreted as recording the very earliest SGFs (muddy turbidity currents) to reach this part of the Indian Ocean.

METHODS/DATA

Core description

Lithological description of the core was made at a centimetre-scale from shipboard observations and post-cruise core photograph analysis (see *Supplementary Information* for details). The dominant lithologies, together with the dominant mineralogical/biological components (terrigenous, biogenic, volcaniclastic and igneous) define the main categories of facies (see McNeill *et al.*, 2017b). Facies classification is based on the scheme of deep-water siliciclastic sediments of Pickering *et al.* (1986), modified in Pickering & Hiscott (2016).

Seismic analysis

This study uses two composite regional south-west/north-east cross-sections compiled from seismic lines 179 BRG06-101–105 (Fig. 1). Seismic reflection data were acquired by the Federal Institute for 180 Geosciences and Natural Resources (BGR, 2007; Germany) research cruise SO-186-2 as part 181 of the SeaCause program (2007) and by the National Centre for Scientific Research (CNRS, 182 2000; France) MD116 cruise and Western Geco (McNeill *et al*., 2016; 2017b). The time–depth conversions developed during the expedition (McNeill *et al*., 2017b) suggest a vertical resolution of *ca* 10 to 15 m.

Age model

Biostratigraphic data

The overall age model for sites U1480 and U1481 (Fig. 1) is defined by major tie points identified using biostratigraphy (Fig. 2; Table 1; compiled from McNeill *et al.*, 2017a; b and Backman *et al*., 2019). Tie points are used to calculate linear sediment accumulation rates (LSAR) and mass accumulation rates (MAR). It should be noted that the tie points are based on the time scale presented by McNeill *et al.* (2017b), and the biostratigraphic data used in IODP drill sites include variable amounts of age–depth uncertainties.

Radiocarbon analysis

The late Pleistocene-Holocene sediment accumulation rate is determined from six radiocarbon ages obtained from the topmost 2 m of holes U1480E and U1480H (Table 3).

Samples were strategically collected in foraminifer-rich mud, interpreted as hemipelagite facies associations (see *Supplementary information* for detailed method).

Flux estimates

Sediment flux is estimated from petrophysical shipboard data and the age model presented in this study (Fig. 2; Table 1; Appendix Tables 4, 5 and 6), which slightly differs from McNeill *et al*. (2017a; b). Mass accumulation rates (MAR, expressed in $g \cdot cm^{-2} \cdot kyr^{-1}$) are calculated for both sites using the equation:

$$MAR = \rho_g \times (1-\Phi) \times LSAR$$

where ρ_g is the grain density; Φ is the porosity of the sediment; LSAR is calculated between two tie points. Grain density (ρ_g) was measured on discrete samples during the expedition (see McNeill *et al.*, 2017b, for detailed methodology).

Following the same methodology, MAR were calculated for IODP Expedition 354 Site U1451 and IODP Expedition 353 Site U1443 (after Clemens *et al.*, 2016; France-Lanord *et al.*, 2016; McNeill *et al.*, 2017a; Appendix Tables 4 and 5). These sites are the most complete and continuous sites in the direct vicinity of the study area.

Channel measurements

Channel dimensions were measured from seismic reflection profiles. Channel width was defined as and measured from crest to crest of the channel below a continuous seismic horizon, i.e. the maximum channel width. Channel depth is the maximum observed depth and is defined as and measured from the maximum width position vertically down to the channel thalweg. Seismic data are in two way time (TWT) and, therefore, depth measurements were converted to depth using the seismic reflection interval velocity data.

The channel area is calculated using the channel width and depth and as a function of the shape of the channel. The 'compound channels' were of trapezoid shape and area was estimated as a trapezium: A = ½(a+b)/h, where 'a' and 'b' are the long and short lengths of the trapezoid (the maximum and base widths of the channel, respectively) and 'h' is the distance between them (the maximum depth of the channel). The 'simple' channels were either of triangular or ellipsoid shape. The area for the triangular-shaped channels was estimated as: A = ½(a.h), where 'a' is the maximum width of the channel and 'h' is the

maximum depth of the channel. The area for the ellipsoid-shaped channels was estimated as: $A = ½(\pi.a.h)$, where 'a' is the maximum width of the channel and 'h' is the maximum depth of the channel.

RESULTS

Facies classification and sedimentary processes

Using the facies classification of Pickering *et al*. (1986), modified in Pickering & Hiscott (2016), 26 individual facies are recognized in cores from sites U1481 and U1480 (Table 3; Figs 2, 3 and 5; Appendix Figs 2 and 3). They are arranged into eight facies associations (FA) according to their dominant lithology and depositional processes. Readers can refer to the *Supporting Information* to access the full description of each facies.

Facies Association 1 (FA1) – Turbidites

Normally graded, moderately to well-sorted, sand to mud beds (couplets) dominate the sedimentary record of the Nicobar Fan (Facies C2.1, C2.2, C2.3, D2.1 and D2.3; Table 3; Fig. 5). Sedimentary structures of these very thin to thick beds contain planar parallel lamination, ripple lamination and convolute bedding. Bioturbation is commonly low to moderate overall but increases upward at a bed scale. Basal contacts are sharp to erosive, while the top contact tends to be gradational to mud(stone). The bases of the beds comprise mica-rich quartzo-feldspathic sand with macroscopic plant debris and locally contain millimetre to centimetre-size rounded mudclasts. These facies are interpreted as turbidites emplaced by turbidity currents that remobilized river-sourced material (after Pickering & Hiscott, 2016). These deposits of turbidity currents are called 'sandy turbidites' (FA1a).

Facies G3.1 is characterized by similar grain-size, grading, sorting, lower and upper contact, sedimentary structures and bioturbation trends to those above. The only difference is the grain composition (indigenous and reworked calcareous nannofossils) and the diagenetic stage (visual evidence of compaction and dissolution). Facies G3.1 is interpreted as biogenic-rich turbidites emplaced by SGFs likely triggered by slope failures on the nearby Ninetyeast Ridge. Beds of Facies G3.1 sit within carbonate-free and terrigenous-free muds of Facies E1.2. This alternation of facies suggests that the seafloor was below the CCD (i.e. carbonate

compensation depth) at the time of deposition; SGFs reworking material deposited above the CCD on the ridge to the west emplaced episodically biogenic-rich turbidites at drill sites. For simplification, Facies G3.1 deposits are called 'calcareous turbidites' (FA1b).

Facies Association 2 (FA2) – Low-concentration turbidites

Normally-graded, moderately to well-sorted, thin to thick-bedded silt and silty-clay is also common in the Nicobar Fan (Facies D2.2, E2.1; Table 3; Fig. 5). Sedimentary structures, bioturbation trends, and top and bottom contacts are comparable to what is observed in the sandy turbidites suggesting that they are genetically related. These facies are interpreted as turbidites emplaced by low-concentration turbidity currents (after Pickering & Hiscott, 2016). In the context of the Nicobar Fan, such flows could be the distal expression of turbidity currents as described above. For simplification, the deposits of low-concentration turbidity currents are called 'muddy turbidites'.

Facies Association 3 (FA3) – Candidate hybrid SGF deposits

These thin to very thick beds are characterized by a crude normal grading, moderate to poor sorting, the common occurrence of convolute bedding in an overall poorly structured deposit, the systematic presence of mudclasts and chips, some plastically deformed, and a wavy to erosive base with common flame structures (Facies C1.1 and D1.2; Table 3; Fig. 5). Bioturbation is low and tends to increase towards the top of beds. The sand-size and silt-size material that comprises these facies is the same as that in the turbidite deposits (mica-rich quartzo-feldspathic sand with macroscopic plant debris). These facies are interpreted as SGF deposits emplaced by so-called 'hybrid SGFs' (*cf*. composite co-genetic flows of Haughton *et al.*, 2009). Those flows can result from the transformation of turbidity currents by an increase in concentration, i.e. bulking up to take on the properties of cohesive flows. In the case of Facies C1.1 and D1.2 that typically occur immediately below candidate hybrid-event beds, flow concentration likely increased by the addition of clay via erosion of the muddy seafloor (possibly supported by the presence of flame structures; Pickering & Corregidor, 2005) and disintegration of soft clasts (i.e. plastically deformed mudclasts). Hereinafter, those deposits that are called 'candidate hybrid event beds'. The beds are referred to as 'candidate' because without perfect preservation of the beds, it is difficult to exclude other processes such as cohesive flow (Pickering & Hiscott, 2016).

A genetic link is suspected between the non-graded, structureless, brecciated muds of Facies E1.4 and the sands and silts of Facies C1.1 and D1.2. Facies E1.4 containing abundant angular mudclasts in a mud matrix that was observed in one case to underlie a sandy turbidite (Facies D2.1 bed). Together they may form a hybrid event bed as described by Haughton *et al.* (2009), although core quality is insufficient to clarify the nomenclature or the sedimentary process (*ibid*.).

Facies Association 4 (FA4) – Hemipelagites

Structureless, non-graded siliciclastic silty-clay to clay of Facies E1.1 and G2.1 is commonly observed alternating with turbidites and candidate hybrid event beds in the Nicobar Fan (Table 3; Fig. 5). They form medium to thick beds with a gradational lower contact and a sharp top. The composition of these facies is dominantly siliciclastic mud with a minor amount of biogenic components. The moderate to intense bioturbation with a moderate to high diversity of species, together with the presence of disseminated ash pods and sand-size foraminifera, all suggest a quiet depositional environment where primary sedimentary structures are homogenized by bioturbation. These facies are interpreted as hemipelagic sediment (hemipelagites of Pickering & Hiscott, 2016); the siliciclastic mud being supplied through river systems and advected by ocean currents and turbidity currents (as nepheloid layers).

Facies Association 5 (FA5) – Pelagites

Structureless, non-graded, highly bioturbated silty-clay to clay of Facies E1.2, G1.1 and G2.2 is characterized by a low terrigenous content (<10%), 10 to 40% of volcaniclastic material and variable amount of calcareous biogenic particles (McNeill *et al.*, 2017b; Table 3; Fig. 5). These facies are interpreted as pelagic sediments (pelagites) emplaced in open-ocean environments (high bioturbation intensity), away from coastal areas and river supplies. The calcareous biogenic particles may reflect either different oceanographic conditions that influenced the development of pelagic organisms and/or differences in depositional depths (i.e. above or below the CCD). Facies G1.1 that includes >50% of calcareous biogenic particles likely accumulated above the CCD in well-oxygenated waters, while Facies E1.2 that is almost devoid of carbonate and alternates with calcareous turbidites was very likely deposited below the CCD. As hypothesized in the facies description (see *Supplementary*

Information), Facies G2.2, which contains 25 to 50% of calcareous biogenic particles and is enriched in volcaniclastic particles, may have accumulated slightly above the CCD.

Facies Association 6 (FA6) – Airfall tephra

Facies H1.1 occurs throughout the Nicobar Fan as normally-graded, well-sorted, structureless, very thin to thick-bedded coarse-grained sand to mud (Table 3; Fig. 5). It commonly shows a lighter colour than the surrounding sediment and bioturbation is restricted to the upper part of beds. These facies, exclusively composed of glass shards, are interpreted as airfall tephra deposits. Facies H1.1 is considered as a secondary product of volcanic activity emplaced on the seafloor by gravity-driven sedimentary processes (i.e. vertical density currents as defined by Manville and Wilson, 2004).

Facies Association 7 (FA7) – Volcanic products

Igneous micro-crystalline rocks of Facies H3.1 and H3.2, as well as the volcaniclastic conglomerate of Facies H2.1, are considered as primary volcanic products with their emplacement directly driven by volcanic activity (Table 3). Facies H3.1 and H3.2 have similar composition, although the shape of crystals and their contact with immediately surrounding sediment suggest different emplacement processes. Facies H3.1 forms thin to thick beds with a homogeneous size of crystals, a common altered glass cap and the presence of 'cooked' sediment underlying the beds, all suggesting a subaqueous lava flow along the seafloor (FA7a; McNeill *et al*., 2017b). In contrast, crystals are coarser in Facies H3.2 and tend to diminish towards the top and bottom of beds. Moreover, both the top and the base of Facies H3.2 are marked by strong recrystallization of the first 20 cm of sediments. Those observations suggest an intrusion within a sediment pile (i.e. a sill or dyke; FA7b).

Facies H2.1, underlying extrusive basaltic lava flows in Unit IV, is interpreted as volcanic breccia deposited immediately prior to an ensuing lava flow over the seabed topography. The high degree of alteration, the highly brecciated nature of the material and the lack of fine-grained matrix, suggest a subaqueous volcanic eruption (FA7a). This hypothesis is strengthened by the presence of highly fractured glass capping the basalts of Facies H3.1, overlying Facies H2.1 in Unit IV.

Facies Association (FA8) – Coring-induced artefacts

Structureless sands and silts of Facies B1.1 and D1.1, as well as parallel-stratified sand of Facies B2.1, are characterized by non-graded, moderately sorted, unconsolidated beds with no bioturbation, a lack of primary sedimentary structures (B1.1 and D1.1) with beds locally delineated by very thin mud beds (B2.1), and the presence of mud and silt clasts (B1.1 and B2.1; Table 3). These facies are mainly observed at the top of cores associated with severe coring disturbance in intervals with low core recovery [Appendix Fig. 2, Appendix Table 2; also for examples of coring-induced sediment deformation, see figs F21 to F26 in McNeill *et al*. (2017b)]. Based on those observations, and because the top boundary of those beds is never recovered, they can be interpreted as truncated sandy turbidites or candidate hybrid event beds. Alternatively, the low core recovery, the high coring disturbance and the sand/silt in the cores where these facies are observed suggest that they are more likely to be coring-induced artefacts in SGF deposits (i.e. disturbed material). In such cases, (pseudo-) parallel stratification was likely created by high rotational strain during the coring process.

Seismic architecture of the Nicobar Fan

The architecture of the Nicobar Fan is evaluated using two regional south-west/north-east cross-sections of the fan that cross-cut U1480 and U1481 drill sites (Fig. 1). Seismic reflectors that image the sedimentary section of the fan are generally thin, subparallel and laterally continuous (Fig. 6). Fourteen reflectors, labelled R1 to R14 from top to base, are well correlated in the Nicobar Fan, extending from the Ninetyeast Ridge to the Sunda subduction front (Figs 1 and 6; Appendix Fig. 4).

Several faults cross-cut these seismic reflectors. Faults have dips of 60 to 75° and dip both to the east and west (e.g. Geersen *et al*., 2015). The majority have normal displacement with evidence for additional strike-slip displacements. Some of them reach the seafloor and are still active, and contribute to the intraplate seismicity in the area (e.g. Delescluse *et al.*, 2012). However, the lack of thick transparent seismic units, large tectonic structures or major unconformites/erosion surfaces suggests a relatively uniform and steady sediment accumulation across the fan.

The detailed analysis of seismic character in the direct vicinity of Site U1480 documents five seismic facies that are correlated to core observations and calibrated in terms of depositional processes (Figs 7 and 8; Table 4):

(i) Seismic Facies S0 comprises deep-submarine channels built and supplied by SGFs. They show various sizes (1 to 15 km wide; 40 to 400 m deep) and seismic characters but are dominantly filled by coarse-grained SGF deposits (Table 4). Channel-fill is aggrading, laterally accreting (compound channels) or single-filled by homogeneous and transparent deposits (simple channels). They are distributed within the fan, but are more common in the shallower sedimentary sections (Fig. 6). The youngest, located east of Site U1480, is a section of the Nicobar Channel (a channel–levée system) that flows between the IODP Expedition 362 sites (Figs 1 and 12A).

(ii) Seismic Facies S1 comprises lobes and lobe complexes identified as lenticular bodies with parallel and laterally discontinuous reflectors (Table 4). Individual lobes are not discernible in seismic, although core material indicates that S1 is characterized by alternating low-energy (muddy turbidites and hemipelagites) and high-energy deposits (sandy turbidites and candidate hybrid event beds). This pattern is compatible with either an episodic and binary activity of the lobes or gradational variations of lobe activity with stacked fining-upward trends.

(iii) Seismic Facies S2 is characterized by an association of lenticular bedding (wider than those of S1) and channels (S0) that form large channel–levée–overbank complexes and/or (associated) lobes (Table 4). Sedimentary facies of S2 appear to be dominated by muddy turbidites, although recovered material might not be representative of the sedimentology of that seismic facies, i.e. unrecovered sands might be part of this seismic facies.

(iv) Seismic Facies S3 comprises inter-lobe, inter-channel and fan fringe deposits characterized by parallel and continuous reflectors (Table 4): S3 is composed of muddy turbidites and/or hemipelagites units of varying thicknesses, with rare, disseminated coarse-grained SGF deposits.

(v) Seismic Facies S4 comprises pre-fan deposits characterized by parallel and continuous reflectors with higher frequency and lower amplitude than other seismic facies (Table

4). They are correlated to the terrigenous-free pelagites and extrusive volcanic deposits of lithological units LU-IIIB and LU-IV.

(vi) Seismic Facies S5 corresponds to the acoustic basement composed of discontinuous and disorganized reflectors of varying frequency and amplitude (Table 4). The acoustic basement shows multiple mound-shaped structures on its top (i.e. seamounts and ridges) that have no significant influence on the structure and continuity of the overlying seismic reflectors. They locally reach the seafloor on the flank of the Ninetyeast Ridge but are generally buried beneath 1 to 3 s TWT of sediment. Facies S5 is reached at 1360 to 1380 mbsf at Site U1480 and comprises both the oceanic crust (LU-VI) and the overlying limestone intruded by a 35 m thick basaltic sill (LU-V).

STRATIGRAPHY OF THE NICOBAR FAN

The Nicobar Fan sedimentary section is divided into three distinct seismic units (SU1 to SU3) sitting above the acoustic basement (SU4; Fig. 6). Unit SU1, bracketed by reflectors R1 and R4, forms a wedge that thickens towards the deformation front forming the trench wedge with onlap terminations of many internal reflectors. Thickness ranges from 0.05 s TWT at Site U1480 near the Ninetyeast Ridge to 1.8 s TWT at the deformation front. Unit SU2, bracketed by reflectors R4 and R12, has homogenous thickness and reflectors remain parallel regardless of distance from the deformation front. In cores, SU1 and SU2 are composed of the complete range of SGF deposits, and all the channels identified in seismic are disseminated within these units. R12 is correlated to the base of LU-IIIA, and SU1 and SU2 constitute the Nicobar Fan *sensu stricto* (Fig. 7). Unit SU3, bracketed by reflectors R12 and R14, has a more variable thickness and blankets the rugose topography of the acoustic basement (R14). In cores, SU3 is correlated to pre-fan deposits devoid of terrigenous material (Seismic Facies S4, pelagite facies). The acoustic basement (SU4) is below reflector R14.

Sediment flux in the Nicobar Fan

Radiocarbon age dating of late Quaternary material of the Nicobar Fan enables improvement of the age model for LU-IA and LU-IB, previously poorly constrained by biostratigraphy, and dating the last occurrence of SGF deposits at Site 1480 (Fig. 4). LU-IA, composed of hemipelagites and tephras, has an LSAR of 20 m/Myr over the last 50 kyr, comparable to the

LSAR of LU-IC that exhibits similar facies (17 m/Myr; Fig. 4; Appendix Fig. 2). Considering a stable LSAR throughout LU-IA, the boundary between LU-IA and LU-IB is dated at *ca* 280 ka, which also corresponds to the last occurrence of SGF deposits in Site U1480. Combined with the biostratigraphic data of McNeill *et al.* (2017b), the LSAR of LU-IB reaches 78 m Myr^{-1}; a reasonable estimate compared to units with similar facies downhole (LU-IIA, LU-IIB and LU-IIC; Fig. 4).

Mass accumulation rates (MAR) calculated from LSAR, grain density and sediment porosity in Site U1480 suggest abrupt variations in the sedimentary dynamics of the Nicobar Fan (Fig. 9; Table 1). LU-II (and LU-IB), characterized by sand-rich SGF deposits, records the highest values (*ca* 10 to 50 $g{\cdot}cm^{-2}{\cdot}kyr^{-1}$), while LU-IA, LU-IC and LU-III, dominated by mud-rich facies, have a MAR one order of magnitude lower (*ca* 0.5 to 5.0 $g{\cdot}cm^{-2}{\cdot}kyr^{-1}$). As evidenced from seismic stratigraphic analysis, no major tectonic activity is recorded in the architecture of the Nicobar Fan (apart from in SU1), and the faults identified in Fig. 6 have little to no impact on the overall stratigraphy. Hence, the observed MAR variations at Site 1480 (from <0.5 to >50 $g{\cdot}cm^{-2}{\cdot}kyr^{-1}$) were controlled by changes in local sedimentary processes, such as the dominance of SGF or hemipelagite deposition, and reflect changes in the location of sediment transport and deposition within the fan since the early Miocene.

An abrupt decrease in linear sediment accumulation rates (LSAR) occurs between R3 and R4, dated at *ca* 1.7 Ma and *ca* 2.1 Ma, respectively (McNeill *et al.*, 2017b; Figs 4 and 7). Below R4, the thickness of SU2–SU3 is relatively uniform and the reflectors are essentially laterally continuous. Above R4, Site U1480 is probably representative of the wider Nicobar Fan, but not of sedimentation closer to the subduction deformation front where the trench wedge is significantly thicker with higher LSARs. In core, the change in LSAR is marked by the boundary between the hemipelagite-rich LU-I and SGF deposit-dominated LU-II. Combining those observations, a major change in sediment depositional processes occurred at *ca* 2 Ma in the Nicobar Fan; likely linked to collisional processes of the Ninetyeast Ridge with the Java Trench, leading to the temporary cutting off of major coarse-grained SGFs into the Nicobar Fan, expressed in the deposition of the pelagites and hemipelagites of LU-IC. This event did not necessarily mark the initial impingement, but rather a time when seafloor topography on the colliding Ninetyeast Ridge impeded SGFs so that they were re-routed onto the Bengal Fan.

DISCUSSION

Depositional history of the Nicobar Fan

Timing of fan activity

The oldest sediments lying on the oceanic crust at 3°N are pelagites dated at *ca* 69 Ma (limestones of LU-V; Fig. 4; Table 1; McNeill *et al.*, 2017b). The pre-fan succession has a complex history with intrusions and extrusions of volcanic material within and between the pelagites. Biostratigraphic data revealed a major *ca* 40.7 Myr hiatus at 1326.39 ± 0.43 mbsf spanning the late Palaeocene through to early Miocene, i.e. from 51.8 to 17.4 Ma (Backman *et al.*, 2019) , possibly located at 1326.71 mbsf where a prominent hardground surface developed (Figs 2 and 10). This significant time gap in stratigraphy does not appear clearly in the seismic data, suggesting a regional extent, at least at the scale of the seismic data used in this study (between R12 and R14 in Fig. 6). The homogeneity of seismic character SU3 in the region, excluding the hiatus, suggests the low MAR recorded in U1480 is representative of the sedimentary dynamics of the Indian Ocean during the early Miocene (0.5 $g{\cdot}cm^{-2}{\cdot}kyr^{-1}$ for the 22 to 19 Myr period; Fig. 9; Table 1). Above SU3, within the siliciclastic succession of the Nicobar Fan, no other comparably large hiatus is recorded. Backman *et al*. (2019) suggested that the cause of this *ca* 41 Myr hiatus may be due to: "*… some combination of changing paleogeographic settings (including paleolatitudinal positions) and deep ocean circulation* …", for example erosion below thermohaline circulation. Another possibility is that it represents repeated sediment failure along low-angle (bedding plane) detachments and sliding on the flanks of the Ninetyeast Ridge at a scale irresolvable by seismic. It could also be a combination of several processes.

The first appearance of terrigenous SGF deposits occurs at 1310 to 1312 mbsf in core U1480G-60R where the facies change uphole from stacked pelagites and calcareous turbidites (i.e. LU-IIIB) to alternating hemipelagites and mud-turbidites (i.e. LU-IIIA; Fig. 2; Appendix Fig. 2). Overall, the bulk mineralogy of mud facies shows an abrupt increase in silt-size to mud-size quartz particles from 2–5% to 15–20% (McNeill *et al.*, 2017b). The

boundary between LU-IIIA and LU-IIIB is dated at *ca* 19 Ma, which corresponds to the oldest siliciclastic turbidites recorded in IODP Expedition 362 sites, and consequently to the initiation of the Nicobar Fan at 3°N. Up to *ca* 9.5 Ma, LU-IIIA accumulates alternating muddy turbidites, hemipelagites and tephra with a low but increasing MAR of *ca* 1 to 3 $g{\cdot}cm^{-2}{\cdot}kyr^{-1}$ in Site U1480. At the same time, in Site U1481, LU-IIIA accumulates similar facies with a basal 20 m thick interval of sandy turbidites and candidate hybrid event beds at slightly higher, but also increasing rates (*ca* 2 to 5 $g{\cdot}cm^{-2}{\cdot}kyr^{-1}$; Fig. 9; Table 1). From *ca* 9.5 Ma, MAR abruptly increase by one order of magnitude correlating with substantial changes in lithologies, facies and architecture of the fan (using reflector R12 as proxy; Figs 2, 6 and 7). Sandy turbidites, candidate hybrid event beds and mud-turbidites then dominate the sedimentary record up to *ca* 2 Ma (i.e. LU-IIC, LU-IIB and LU-IIA). The 9.5 to 2.0 Ma period is characterized by high MAR that shows a sinusoid-like trajectory with peaks at 9.2 to 8.3 Ma and 2.4 to 2.0 Ma (43 and 53 $g{\cdot}cm^{-2}{\cdot}kyr^{-1}$, respectively) and a minimum at 5.2 to 3.8 Ma (10 $g{\cdot}cm^{-2}{\cdot}kyr^{-1}$; Fig. 9). However, the authors note that these details are reliant on the tie point positions of the age model. The abundance and area of channels show a similar trend to the MAR at Site U1480, increasing between LU-IIB and LU-IIA, which suggests comparable sedimentation patterns across the fan.

Sediment supply significantly decreased at *ca* 2 Ma (reflector R4, at SU1) in Site U1480 and dropped further at *ca* 1.7 Ma (reflector R3 in Fig. 6) with the deposition of mud-rich facies (LU-IC); however, sediment continued to be added to the trench wedge from this time, creating an accumulated sediment thickness of up to 1500 to 2000 m, including channels. The trench wedge material is probably a combination of sediment derived directly from the fan via along-axis transport and sediment reworked from the subduction forearc; however, the relative proportions remain unknown (SU1; Fig. 6). The *ca* 13 m thick turbidite-rich LU-IB in Site U1480, that lasts 150 kyr from 0.43 to 0.28 Ma, is more likely to represent a truncated record of SU1 rather than a condensed section of the trench wedge (Fig. 4; Appendix Fig. 2). However, questions remain about the representativeness of the hemipelagite units LU-IC and LU-IA dated at 1.7 to 0.43 Ma (1.7 to 0.8 Ma if the low MAR at the top of LU-IC is attributed to basal erosion of LU-IB; Fig. 5) and 0.28 to 0 Ma.

Holocene activity of the Nicobar Fan is restricted to small volume and isolated SGFs that originate from local, small-scale destabilizations of the Sunda forearc and accretionary

prism; otherwise most of the fan is covered by hemipelagic deposits (Bandyopadhyay & Bandyopadhyay, 1999; Tappin *et al.*, 2007; Sumner *et al.*, 2013; Patton *et al.*, 2015). The Nicobar Channel that flows southward between the IODP Expedition 362 sites is currently inactive and blanketed by *ca* 5 m of hemipelagic deposits as revealed by cores collected in the channel axis (Fig. 1; RR0705 Superquakes07 Cruise Report) and on the levées (this study). According to the results of IODP Expedition 362 (Site U1480), the Nicobar Channel is likely to have been inactive since *ca* 280 ka.

Provenance

Terrigenous material recorded in the Nicobar Fan composed of micaceous quartzo-feldspathic material (mostly turbidites) points to a continental origin, and the very abundant macroscopic plant debris and coal fragments recorded in sites U1480 and U1481 suggest a strong river influence (McNeill *et al.*, 2017b). Preliminary compositional and provenance analyses of Nicobar Fan sediments show a uniform and homogenous assemblage of transported sedimentary material since *ca* 19 Ma, derived from the Greater and Tethyan Himalaya mixed with sediment from the Burmese arc-derived Palaeogene Indo–Burman Ranges (McNeill *et al.*, 2017a; b). Nicobar Fan sediments and turbidites are therefore very similar in source to those recorded in the Bengal Fan, which confirms the hypothesis that the Bengal Fan and the Nicobar Fan are part of the BNFS and are dominantly fed by the Ganges-Brahmaputra River system that drains the central and eastern Himalaya Range (Curray, 2014, and references therein; France-Lanord *et al.*, 2016).

Many southward-flowing Quaternary and buried channels are identified on bathymetry and in seismic data of the BNFS (Curray *et al.*, 2003; Schwenk & Spiess, 2009; Fournier *et al.*, 2017, McNeill *et al.*, 2017b; this study). In the Bengal Fan, the Bengal Channel has been active in the Holocene and supplies the western side of the fan, delivering sediments from the 'Swatch Of No Ground Canyon' in the Bay of Bengal (20°N) southward to ODP Leg 116 sites 717 to 719 (2°S; Fig. 1). In the Nicobar Fan, the Nicobar Channel is at least 1500 km long extending from 9°N down to 5°S (Fig. 1). Its northern termination is unclear, although the recent efforts of Jena *et al.* (2016) to synthesize and refine available bathymetry data in the eastern side of the Bengal Fan show that channels E6 and E7 of Curray *et al.* (2003), that flow south-east on the upper and middle Bengal Fan, merge at 10.64°N. They form a channel

flowing southward east of the Ninetyeast Ridge that likely becomes the Nicobar Channel in the Nicobar Fan (Fig. 1; Jena *et al.*, 2016). Channels E6 and E7 were active in the Pleistocene (Curray *et al.*, 2003), which means that the Ganges–Brahmaputra River system directly supplied the Nicobar Fan in the Quaternary.

Sandy and muddy turbidites are the most common facies in upper units (LU-I to LU-IIIA) and form the sandy Nicobar Fan *sensu stricto*, while they are absent in the older pre-fan units (LU-IIIB to LU-VI) composed of hemipelagites, pelagites and igneous rock facies. In LU-IIIB, the bulk mineralogy as determined by X-ray diffraction (fig. F6, McNeill *et al.*, 2017b) shows comparable quartz and feldspar content to the younger sandy parts of the Nicobar Fan, and also contains intercalated siltstones (for example, fig F26, *ibid*.).

Abandonment of the Nicobar Fan

The last activity of the Nicobar Channel as recorded in Site U1480 (LU-IB) is dated at *ca* 430 to 280 kyr (Fig. 4; Appendix Fig. 2). This provides more specific timing information whilst generally supporting the mid Pleistocene timing previously proposed (Curray & Moore, 1974; Curray *et al.*, 2003). In the Bengal Fan, the most recent fan activity (125 to 0 ka) appears restricted to the western side of the fan, although from 425 to 125 ka, the sediment supply switched to the eastern side feeding E6 and E7, and therefore the Nicobar Channel (Curray *et al.*, 2003).

The most likely cause for the abandonment of the Nicobar Fan was either: (i) cut off from the Bengal Fan due to impingement of the Ninetyeast Ridge with the subduction zone leading to topographic obstruction of the feeding channels; or (ii) large-scale avulsion of the Bengal-Nicobar Fan in the Bay of Bengal *before* the collision, resulting in funnelling of the sediment supply to the western side of the fan (i.e. the Bengal Fan). Either process would have been associated with fan-scale avulsion processes. The former hypothesis was proposed in the earliest exploration stages of the BNFS (Curray & Moore, 1974), subsequently endorsed by seismic stratigraphy (Curray *et al.*, 2003; Schwenk & Spiess, 2009) and drilling results that provided continuous sedimentary records since the middle Eocene (Cochran *et al.*, 1989; 1990; Peirce *et al.*, 1989; Stow *et al.*, 1990; France-Lanord *et al.*, 2016). The latter hypothesis is supported by the timing of activity within the E6 and E7 channels and their connection to the Nicobar Fan, as demonstrated by recent drilling (McNeill *et al.*, 2017a; b; this study) and

bathymetry results (Jena *et al.*, 2016) in the hitherto poorly studied Nicobar Fan. Therefore, the combined effects of both allogenic (collision of the Ninetyeast Ridge) and autogenic factors (late Quaternary avulsion in the upper Bengal Fan) may have both contributed to the abandonment of the Nicobar Fan. A more focussed analysis of bathymetric and seismic data available in the northern edge of the Nicobar Fan, where the Ninetyeast Ridge abuts the Sunda margin, may help to unravel the mechanism(s) that led to cut off of the sediment supply during the Quaternary.

Implications for the understanding of the Bengal–Nicobar depositional system

The deep-marine part of the modern BNFS comprises the Bengal Fan and the Nicobar Fan (Fig. 1). The architecture of the Bengal Fan is assessed from a west–east 470 km long transect at 8°N that includes Site U1451 (seismic profile GeoB97-020/027; Schwenk & Spiess, 2009). In the present study, the interpretations of Schwenk & Spiess (2009) were updated using core data from Site U1451 (in France-Lanord *et al.*, 2016; Appendix Fig. 5). This profile is considered representative of the sedimentation dynamics of the Bengal Fan (LSAR comparable to sites 717–719; Schwenk & Spiess, 2009; McNeill *et al.*, 2017b). The Bengal Fan transect is then compared here to the 300 km long cross-section of the Nicobar Fan presented in this study (Figs 9 and 11; Appendix Figs 4 and 5).

Seismic architecture

Unconformities

Early studies of the Bengal Fan based on low resolution seismic data identified two regional unconformities (Curray & Moore, 1971; von der Borch *et al.*, 1974; Moore *et al.*, 1974; Curray *et al.*, 2003): a Palaeocene–Eocene 'lower' unconformity that was interpreted to record the India–Asia collision, and a late Miocene 'upper' unconformity of unknown origin. High resolution seismic data presented by Schwenk & Spiess (2009) revealed the late Miocene unconformity was an artefact due to seismic resolution, although two other unconformities were proposed: a Pliocene (4.8 Ma), and a Pleistocene (0.64 Ma) unconformity. These authors attribute these unconformities to local intraplate deformation. The fact that these unconformities are not clearly identified in the Nicobar Fan is consistent with this local-origin hypothesis (Fig. 11).

The 'lower' unconformity, also identified by Schwenk & Spiess (2009), corresponds to a hiatus separating the pre-collision and the post-collision sediments, and to the initiation of SGFs that built the Bengal Fan (Curray *et al.*, 2003). Starting in the early Eocene, this hiatus is apparently contemporaneous with the Eocene–Oligocene hiatus recorded in the pre-fan deposits on the Nicobar Fan, at Site U1480 (Figs 4 and 10).

Channels

Modern channels at the seafloor are a common feature on the Bengal Fan, but rare on the Nicobar Fan. However, buried submarine channels are common in the Nicobar Fan (Fig. 12). Where seismic resolution is sufficiently high, buried channels within the Bengal Fan exhibit well-developed levée–overbank complexes (Schwenk & Spiess, 2009); whereas equivalent channels within the Nicobar Fan, at the latitude of this study, have less well-developed or no discernible levées (Fig. 12), which is suggestive of greater flow confinement. Within the BNFS, the size of channels (excluding levées) varies between the Bengal and Nicobar Fan, probably because of a complex interplay between proximal and distal positions that have been studied, the scale of the fan systems, and seafloor gradients. In the Bengal Fan, channels are *ca* 2 to 60 km wide and 0.08 to 0.25s TWT (*ca* 80 to 250 m, using a velocity of 2 km s^{-1}, see Schwenk and Spiess, 2009) deep, whereas in the Nicobar Fan they are *ca* 2 to 20 km wide and *ca* 10 to 270 m. Thus, overall, width:depth ratios of Bengal Fan channels are larger than those on the Nicobar Fan.

Within the Nicobar Fan, channels can be defined as either simple relatively small channels (one-third of all observed channels) or larger compound channels (two-thirds of the channels) containing stacked and migrated smaller channels within them (Fig. 12). Indeed, some channels show candidate lateral accretion packages (LAPs) that could represent lateral migration of the channels (for example, Fig. 12A). A graph of channel width versus depth for both compound and simple channels on the Nicobar Fan shows wide scatter with a relatively low correlation coefficient, but with the best-fit line suggesting a characteristic width:depth of *ca* 1:30 (Fig. 13A). Figure 13B, showing width:depth versus frequency shows a range from 5 to 140, with a peak of *ca* 30 (Fig. 13B). Unsurprisingly, the compound channels show the largest cross-sectional areas (Fig. 13C). In the Nicobar Fan, channel area ranges from 4 $x10^3$ to 2 x 10^6 m^2, with a mean of 2 x 10^5 m^2 (Fig. 13C). In both fans, channel abundance generally

increases upward from the late Miocene onward (Figs 13C and D). Specifically within the Nicobar Fan, channel size/area and abundance peaks within subunit IIA (*ca* 2 to 3 Ma), but with a distinct low in IIB (3 to 7 Ma) (Figs 13A, 13C). Interestingly, the intervening Subunit IIB (*ca* 440 to 785 mbsf at Site U1480) was a time interval of reduced LSARs with the greatest decrease towards the top of this subunit, where it fell from *ca* 222 m Myr^{-1} to *ca* 65 m Myr^{-1}, before picking up again to 290 + 35 m Myr^{-1} (*cf*. fig. 7 in Backman *et al*., 2019). In the absence of better core recovery of the sands at Expedition 362 sites, the simplest interpretation of this data is that the lower LSARs in Subunit IIB correlate with reduced coarse clastic flux to the Nicobar Fan, and a commensurate reduced ability of the SGFs to erode channels.

No extensive channel has been identified on the seafloor of the Sunda-Sumatra trench from 5°N to 9°S (i.e. the eastern edge of the Nicobar Fan; Moore *et al*., 1982; Patton *et al*., 2015; Sumner *et al*., 2013). As opposed to classical models (Underwood & Bachman, 1982; Lewis, 1994), the trench axis here is not a major sediment pathway, at least during the latest Quaternary. However, many buried Pleistocene channels are observed in the trench wedge offshore North Sumatra (i.e. SU1; Figs 6 and 12) that may represent extensive axial channel systems in the past. The location of the most recent Nicobar Channel away from the trench may be explained by local topography driving avulsion (Jena *et al*., 2016).

Stratigraphic units

The middle Pleistocene to recent trench wedge of the Nicobar Fan shows a more homogenous and a better preserved sedimentary record than the one in the Bengal Fan, the latter being characterized by many local thickness changes and internal unconformities inherited from local tectonic events (Curray *et al*., 2003; Schwenk & Spiess, 2009). Late Miocene to early Pleistocene sedimentary sections are better preserved in the Nicobar Fan, whilst the Bengal Fan contains a more complete record of late middle Miocene successions (Fig. 11). The origin and provenance of the material in the present-day trench wedge (middle Pleistocene to recent), as part of the Nicobar Fan, needs to be ascertained to more fully understand the sedimentary dynamics of the BNFS. The trench wedge likely contains reworked Himalaya-derived material from the accretionary prism. However, if it contains a considerable component of directly-derived Himalaya material, the expanded Quaternary

section of the Nicobar Fan trench wedge could contain an important record for reconstructing the history of the BNFS.

Sediment accumulation patterns

The MAR of Nicobar Fan sites are compared to Bengal Fan (U1451; France-Lanord *et al.*, 2016) and Ninetyeast Ridge sites (U1443; Clemens *et al.*, 2016; Figs 1 and 9), building on McNeill *et al*. (2017a). In an attempt to highlight lateral variability in sediment accumulation in the Bengal Fan, Schwenk & Spiess (2009) evaluated the LSAR for three seismic units from a 470 km long east–west transect at latitude 8°N (seismic line GeoB97-020/027; Fig. 11). These authors show that LSAR observed at Site U1451 is *ca* 75% of the maximum values recorded for the late Miocene unit (*ca* 13.5 to 5.33 Ma), *ca* 40% for the Pliocene unit (5.33 to 1.8 Ma) and *ca* 30% for the Pleistocene unit (1.8 to 0 Ma). These uncertainties are reported in Fig. 9.

Since the Middle Miocene, the Nicobar Fan has been a major area of sedimentation east of the Ninetyeast Ridge (McNeill *et al.* 2017a). Ninetyeast Ridge Site U1443, characterized by deposition of nannofossil ooze and chalk with clay and volcanic ash (Clemens *et al.*, 2016), is devoid of terrigenous SGF deposits, although the flows running through the Nicobar Fan since late Miocene likely created nepheloid layers that deposited various muddy facies. The abrupt increase in sediment supply in the Nicobar Fan at 9.5 to 2.0 Ma was coeval with an increase in terrigenous clay and a doubling of MAR in Site U1443 on the Ninetyeast Ridge. When sediment supply was reduced in the Nicobar Fan from *ca* 2 Ma onward, MAR on the Ninetyeast Ridge also reduced, more specifically *ca* 1 Ma, recovering to 'typical' values of 0.5 to 0.6 $g{\cdot}cm^{-2}$ kyr^{-1} (Fig. 9; Table 1; McNeill *et al.*, 2017a).

The regional correlation of MAR in the BNFS between 8°N to 3°N shows a period of extremely low MAR at 15 to 18 Ma (or possibly 15 to 19 Ma), with values of one order of magnitude below normal (Fig. 9). This apparent hiatus, or condensed section, is not clearly recognized in cores or seismic data (Schwenk & Spiess, 2009; Curray *et al.*, 2014; Clemens *et al.*, 2016; France-Lanord *et al.*, 2016; McNeill *et al.*, 2017b). Only Site U1453 records a change in sedimentological character at this time, as this hiatus correlates with an anomalous interval enriched in authigenic carbonate by a factor of six (Clemens *et al.*, 2016).

The Bengal and Nicobar fans both show similar trends in MAR since the middle Miocene (Fig. 9). Mass accumulation rates (MAR) follow a sinusoid-like trend with peaks in sediment supply during the late Miocene (*ca* 9.5 to 8.2 Ma, extending to *ca* 7 Ma on the Nicobar Fan) and Pleistocene (2.4 to 2.0 Ma in the Nicobar Fan; 2 to 0 Ma in the Bengal Fan). The lowest sediment supply was in the early-middle Miocene (*ca* 18.0 to 12.5 Ma) and in the early Pliocene (5.5 to 3.6 Ma). This trend in sediment accumulation patterns is also comparable to the Indus Fan sedimentary record (Clift *et al.*, 2008), suggesting regional controls (tectonics and/or climate) on sediment supply related to uplift and denudation of the Himalaya Range. The Pleistocene peaks in MAR in the Bengal and Nicobar fans are coeval with a peak in MAR is also recorded in the Indus Basin (Métivier *et al.*, 1999), and together correlate with the acceleration of denudation rates and sediment transport observed in the Himalaya Range since *ca* 2 Ma (up to a factor of four; Herman *et al.*, 2013). Similar net increases in denudation and transport may explain the late Miocene peak (*ca* 7 to 10 Ma) in accumulation rates observed in the BNFS, although that increased MAR is delayed as compared to the higher values one recorded in the Indus Fan, which occurred at *ca* 10 to 16 Ma (Clift *et al.*, 2008). The apparent delay in sedimentary record between the Indus Fan and the BNFS may be explained by local tectonic conditions (i.e. Sunda Subduction) that diverted the sediment supply to the eastern side of the BNFS (i.e. trench axis), and this earlier material is now part of the Sunda accretionary prism (Fig. 14).

Palaeogeographic reconstructions

The observations and analyses undertaken on IODP Expedition 362 sites and presented in this paper are integrated with results from DSDP (Leg 22; von der Borch *et al.*, 1974), ODP (Leg 116 and 121; Cochran *et al.*, 1989; Peirce *et al.*, 1989) and other IODP sites (Expeditions 353 and 354; Clemens *et al.*, 2016; France-Lanord *et al.*, 2016) to reconstruct the depositional history of the BNFS using the Palaeogene–Neogene reconstructions of the Indian Ocean of Hall (2012) (Figs 1, 9 and 14), and building on McNeill *et al*. (2017a).

During the late Pleistocene to present (0 Ma map; Fig. 14), sediments supplied by the Ganges–Brahmaputra River system were delivered to the Bengal Fan via a series of submarine channels preserved on the modern seafloor (Curray *et al.*, 2014; Fig. 1). Site U1451 records an average MAR of *ca* 70 $g{\cdot}cm^{-2}{\cdot}kyr^{-1}$, while Site U1480 records hemipelagic

deposits with low MAR (*ca* 1 $g{\cdot}cm^{-2}{\cdot}kyr^{-1}$). During the Pliocene and early Pleistocene (5 Ma map; Fig. 14), sediment supply was mainly directed to the Nicobar Fan, likely due to fan-scale avulsion processes and/or the presence of an eastern (channelized) pathway through the Ninetyeast Ridge before its collision/impingement with the Sunda subduction zone. The Nicobar Fan records an average MAR of *ca* 20 to 50 $g{\cdot}cm^{-2}{\cdot}kyr^{-1}$, while the Bengal Fan records a reduced but persistent terrigenous signal (MAR of *ca* 5 to 10 $g{\cdot}cm^{-2}{\cdot}kyr^{-1}$). This time period includes an interval of reduced sediment supply in the early Pliocene for both the Bengal and Nicobar fans followed by overall increasing sediment flux to the Nicobar Fan during the late Pliocene to early Pleistocene (Fig. 9), with four to five times more sediment accumulation recorded in the Nicobar Fan (10 versus 2–3 $g{\cdot}cm^{-2}{\cdot}kyr^{-1}$ Fig. 9). In the late Miocene (10 Ma map; Fig. 14), the Bengal Fan was the main depocentre for sediment accumulation (MAR of *ca* 20–30 $g{\cdot}cm^{-2}{\cdot}kyr^{-1}$). However, an unknown portion was likely funnelled into the Sunda trench, bypassing the Nicobar Fan that had low MAR at that time (*ca* 3–5 $g{\cdot}cm^{-2}{\cdot}kyr^{-1}$), crossing the Investigator Ridge and contributing to the deposition of SGF-deposit units in Site 211 to form a southern fan, here named the 'Investigator Fan' (Figs 1 and 14). During the middle Miocene (15 Ma map; Fig. 14), the Bengal Fan still received a significant part of the sediment volume (in Site 718; McNeill *et al.*, 2017a), although palaeogeographic reconstructions suggest that the Sunda Trench may by this time be the main sink for Himalaya-derived material (McNeill *et al.*, 2017a). The Nicobar Fan preserves only distal muddy SGF deposits (MAR of *ca* 1–2 $g{\cdot}cm^{-2}{\cdot}kyr^{-1}$). The Investigator Fan likely preserves the lateral margin to the Nicobar Fan at this time, with the more axial parts of the fan having been incorporated into the forearc accretionary prism. From the early Miocene (20 Ma map) to the early Oligocene (30 Ma map), as the Indo-Australian Plate moved south, the Bengal and Nicobar fans were progressively disconnected from the proto-BNFS as their distance from the proto-Ganges–Brahmaputra river increased (Fig. 14). The oldest turbidites recorded in the western part of the Nicobar Fan are late Miocene (this study), and probably older in the eastern side or within now accreted parts of the fan. In the Bengal Fan they are early Oligocene (Curray *et al.*, 2014).

Palaeogeographic reconstructions show that most of Oligocene and Miocene sediments, and therefore the sedimentary record of Himalaya uplift and denudation, now constitutes the accretionary prism of the Sunda subduction margin (Fig. 14; Curray *et al.*, 1979; Karig *et al.*,

1980; Pal *et al.*, 2003; Bandopadhyay & Glosh, 2015). In the Andaman and Nicobar islands, the latest Eocene and early Oligocene time interval is marked by the abundant supply of deep-marine siliciclastic material (Andaman Flysch) that accumulated as extensive and thick sandy SGF deposits, mostly turbidites, in submarine-fan environments (Bandopadhyay & Carter, 2017; Limonta *et al*., 2017; Bandopadhyay & Carter, 2018). These sediments accumulated in a palaeo-Sunda trench and were subsequently accreted to the Sunda Arc as accretionary-prism material (Bandopadhyay & Carter, 2018). Estimates of the thickness of the Andaman Flysch range from 750 m (Roy, 1983) to 3000 m (Pal *et al*., 2003). Regarding sediment provenance, Limonta *et al*. (2017) present the most extensive coverage of samples to date from the Andaman Flysch, and make the point that all sandstone samples (western region of Andaman and Nicobar islands) show clear affinities with the Bengal Fan, apart from the 'Corbyns Cove section' (eastern Andaman) which has some heavy mineral and petrological characteristics that might represent an Irrawaddy or Burma margin input (graph D in fig. 10.7). However, the detrital zircon data (graph C in fig. 10.7) do not show this link. Bandpoadhyay & Carter (2017) examine Corbyns Cove sandstone geochemistry and argue that it is slightly different from the other Andaman Flysch samples in that there is a higher portion of young arc material, an observation that could fit with a sediment contribution from the Burmese margin rather than the Irrawaddy River *per se* or an arc to the west. A problem for any significant Irrawaddy River contribution to the Nicobar Fan is posed by the uplifted crustal blocks of the Sewell Rise and Alcock Rise that mark the western side of the East Andaman Basin (see fig. 1 in Srisuriyon & Morley 2014).

At Expedition 362 Site U1480, terrigenous input began in the early Miocene at *ca* 22.5 Ma as muds, with very thin-bedded and thin-bedded muddy turbidites at *ca* 19.5 Ma. From 9.5 Ma, sand content and sediment supply sharply increase. Indeed, from the late Miocene, the BNFS (i.e. the Bengal, Nicobar and Investigator fans) formed the main depositional sink for Himalaya-derived material. To obtain the most complete sedimentary record of Himalaya uplift and denudation, one must consider the BNFS in its entirety and not focus on one fan alone, and in terms of sediment volumes, should not neglect the material accreted to the Sunda forearc (*cf*. McNeill *et al.*, 2017a). Figure 14 shows the occurrence of several large-scale avulsion events within the BNFS that make each fan the dominant sink at different

times: the Bengal Fan during the late Pleistocene and late Miocene, the Nicobar Fan during the Pliocene to early Pleistocene and the Investigator Fan during the late Miocene.

CONCLUSIONS

In spite of any age uncertainties in the datasets involved (Curray *et al.*, 2003; this study), the sedimentological, compositional and stratigraphic evidence all confirm that the Nicobar Fan is part of the sedimentary record of the uplift and denudation of the Himalaya Range, and is an important part of the Miocene to recent tectono-stratigraphic record for the north-east Indian Ocean and adjacent areas.

The Nicobar Fan can be classified as a mud-dominated fan system, similar to the neighbouring Bengal Fan. Dated at *ca* 19 Ma, the base of LU-IIIA marks the beginning of the influx of siliciclastic sediment gravity-flow (SGF) derived sand to the Nicobar Fan, although the earliest record of fan deposition may be the first occurrence of terrigenous mudstones dated at *ca* 22.5 Ma (Fig. 9, LU-IIIB). Candidate earliest fan, and pre-fan deposits (69 to 19 Ma; LU-IIIB to LU-VI) are characterized by extremely slow accumulation of hemipelagites and pelagites (0.5 $g{\cdot}cm^{-2}{\cdot}kyr^{-1}$), with the common occurrence of lava flows and basaltic intrusions. A major hiatus, contemporaneous with the Palaeocene to Eocene lower unconformity within the Bengal Fan, is recognized in the Nicobar Fan at 1326.71 mbsf at Site U1480 (58.1 to 17.4 Ma), but cannot be identified in seismic data. From *ca* 19 Ma to *ca* 2 Ma, sediment accumulation is relatively uniform across the Nicobar Fan (LU-II to LU-IIIA), however accumulation rates increased abruptly at *ca* 9 Ma. Fluctuations in mass accumulation rate (MAR) from Site U1480 (10 to 50 $g{\cdot}cm^{-2}{\cdot}kyr^{-1}$) are considered representative of the fan dynamics for this time period. From the early Pleistocene to present (*ca* 2 to 0 Ma; LU-I), the depositional history of the Nicobar Fan is unclear. Part of its depositional history may be contained in the expanded Quaternary record of the trench wedge, not drilled in IODP Expedition 362.

The Nicobar Fan is currently inactive as shown by the *ca* 5 m thick hemipelagic drape identified throughout the fan and across the Sunda trench. Fan abandonment is dated at *ca* 0.28 Ma at Site U1480 (base of LU-IA), which represents the last activity of the southward

flowing Nicobar Channel. Recent studies suggest that the Nicobar Channel was connected to the Bengal Fan in the Quaternary and therefore directly fed by the Ganges–Brahmaputra River System. Geochemical and compositional analyses also argue for Himalayan-derived origins of Nicobar Fan sediments.

The temporal evolution of sediment supply in the Bengal–Nicobar Fan System (BNFS; i.e. the Bengal Fan and the Nicobar Fan) shows intriguing variations at a million-year timescale: the BNFS overall records two peaks in MAR in the late Miocene (9.2 to 8.3 Ma) and the Pleistocene (2.4 to 0 Ma) separated by a low in the late Miocene–Pliocene (5.5 to 3.6 Ma). This regional fluctuation in sediment supply matches that of the Indus Fan and may highlight regional climatic and/or tectonic changes. Palaeogeographic reconstructions of the BNFS show that much of the Oligocene and Miocene Himalayan-derived material is now stored in the accretionary prism of the Sunda subduction margin and that the Bengal, Nicobar and Investigator fans only provide a representative sedimentary record from the late Miocene onward. Short-scale variations in MAR and the constituent facies and facies associations record large-scale avulsion processes that alternatively favoured one fan (Bengal, Nicobar or 'Investigator') into which SGF deposits preferentially accumulated. This integrated analysis of the BNFS has revealed that most of the SGFs are directed towards the Bengal Fan and the 'Investigator Fan' in the mid–late Miocene, to the Nicobar Fan in the late Miocene to early Pleistocene, and to the Bengal Fan in the late Pleistocene. A vision of a heterogeneous sedimentation within the BNFS, with change occurring spatially rather than simply temporally, is critical for a reliable analysis of the sedimentary record to investigate the interplay of climate and tectonic processes on the uplift and denudation of the Himalayas, and for improving current understanding the dynamics of large submarine fan systems.

ACKNOWLEDGEMENTS

This research used samples and data provided by the International Ocean Discovery Program (IODP) (www.iodp.org/access-data-and-samples). We thank the *JOIDES Resolution* crew and IODP technical team for their support during IODP Expedition 362. The entire IODP Expedition 362 science party are thanked for their contributions to the data used here. Seismic data used here were acquired by the Federal Institute for Geosciences and Natural

Resources (BGR), Germany; data are jointly owned by German and Indonesian institutions, and we thank Christoph Gaedicke for data access. Esther Sumner is thanked for helping with the section on submarine channels. Pouderoux acknowledges support by CNRS and IODP France before, during and following the expedition from a postdoctoral grant (A64622) and a post-cruise financial support from IODP France. The authors are grateful for the work and support of the editorial board of Sedimentology, and for the constructive reviews of Ian Kane (editor), Hannah Brooks, Menno Hofstra and Ben Kneller (reviewers) that contributed to the improvement of the manuscript.

REFERENCES

Backman, J., Chen, W., Kachovich, S., Mitchison, F., Petronotis, K., Yang, T. and Zhao, X. 2019. Data report: revised age models for IODP Sites U1480 and U1481, Expedition 362. *In*: McNeill, L.C., Dugan, B., Petronotis, K.E. and the Expedition 362 Scientists, *Sumatra Subduction Zone, Proceedings of the International Ocean Discovery Program*, **362**. College Station, Texas (International Ocean Discovery Program). https://doi.org/10.14379/iodp.proc.362.202.2019

Bandopadhyay, P.C. and Carter, A. 2017. Geological framework of the Andaman–Nicobar Islands. *In*: Bandopadhyay, P.C. and Carter, A. (eds), *The Andaman–Nicobar Accretionary Ridge: Geology, Tectonics and Hazards*. Geological Society, London, Memoirs, **47**, 75–93.

Bandopadhyay, P.C. and Ghosh, B. 2015. Provenance analysis of the Oligocene turbidites (Andaman Flysch), South Andaman Island: a geochemical approach. *Journal of Earth System Science*, **124**, 1019–1037.

Bandyopadhyay, A. and Bandyopadhyay, R.R. 1999. Subsea channels and incidence of thermogenic hydrocarbons in the mid-proximal Bengal Fan, west of the Andaman-Nicobar Islands. *Marine Georesources and Geotechnology*, **17**, 1–16.

Bastia, R., Das, S. and Radhakrishna, M. 2010. Pre- and post-collisional depositional history on the upper and middle Bengal fan and evaluation of deepwater reservoir potential along the northeast Continental Margin of India. Marine and Petroleum Geology, **27**, 2051–2061.

Bourillet, J-F., Damy, G., Dussud, L., Sultan, N. and Woerther, P. 2007. Behavior of a piston corer from accelerometers and new insights on quality of the recovery. Proceedings of the 6th International Offshore Site Investigation and Geotechnics Conference: Confronting New Challenges and Sharing Knowledge, 11–13 September 2007, London, UK.

Clemens, S.C., Kuhnt, W., LeVay, L.J. and the Expedition 353 Scientists, 2016. Indian Monsoon Rainfall. *Proceedings of the International Ocean Discovery Program*, **353**. College Station, Texas (International Ocean Discovery Program). http://dx.doi.org/10.14379/iodp.proc.353.2016.

Clift, P., Hodges, K.V., Heslop, D., Hannigan, R., Van Long, H. and Calves, G. 2008. Correlation of Himalayan exhumation rates and Asian monsoon intensity. *Nature Geoscience*, **1**, 875–880.

Clift, P.D. 2002. A brief history of the Indus River. *In*. Clift, P.D., Kroon, D., Gaedicke, C. and Criag, J. (eds), *The Tectonic and Climatic Evolution of the Arabian Sea Region*. Geological Society, London, Special Publications, **195**, 237–258.

Clift, PD., Shimizu, N., Layne, G.D., Blusztajn, J.S., Gaedicke, C., Schlüter, H-U., Clark, M.K. and Amjad, S. 2001. Development of the Indus Fan and its significance for the erosional history of the Western Himalaya and Karakoram. *Geological Society of America Bulletin*, **113**, 1039–1051.

Cochran, J.R., Stow, D.A.V., *et al.* 1989. Leg 116 Distal Bengal Fan. Proceedings of the Ocean Drilling Program, Initial Report, vol.116. Ocean Drilling Program, College Station, TX. http://dx.doi.org/10.2973/odp.proc.ir.116.1989.

Cochran, J.R., Stow, D.A.V., *et al.* 1990. Leg 116 Distal Bengal Fan. Proceedings of the Ocean Drilling Program, Scientific Results, vol.116. Ocean Drilling Program, College Station, TX. http://dx.doi.org/10.2973/odp.proc.sr.116.1990.

Covault, J.A. and Graham, S.A. 2010. Submarine fans at all sea-level stands: tectono-morphologic and climatic controls on terrigeneous sediment delivery to the deep sea. *Geology*, **38**, 939–942.

Curray, J.R. 2014. The Bengal Depositional System: from rift to orogeny. *Marine Geology*, **352**, 59–69.

Curray, J.R. and Moore, D.G. 1971. Growth of the Bengal Deep-Sea Fan and Denudation in the Himalayas. *Geological Society American Bulletin*, **82**, 563–572.

Curray, J.R. and Moore, D.G.. 1974. Sedimentary and tectonic processes in the Bengal deep-sea fan and geosyncline. *In*: Burk, C.A.. and Drake, C.L. (eds), *Continental Margins*, 617–627. Springer, New York.

Curray, J.R., Emmel, F.J. and Moore, D.G. 2003. The Bengal Fan: morphology, geometry, stratigraphy, history and processes. *Marine and Petroleum Geology*, **19**, 1191–1223.

Curray, J.R., Moore, D.G., Lawver, L.A., Emmel, F.J., Raitt, R.W., Henry, M. and Kiekheffer, R. 1979. Tectonics of the Andaman Sea and Burma. In. Watkins, J., Montadert, L., Dickerson, P.W. (eds). Tectonics of the Andaman Sea and Burma. *American Association of Petroleum Geologists, Memoir*, **29**, 189–198.

Delescluse, M., Chamot-Rooke, N., Cattin, R., Fleitout, L., Trubienko, O. and Vigny, C. 2012. April 2012 intra-oceanic seismicity off Sumatra boosted by the Banda-Aceh megathrust. *Nature*, **490**(7419), 240–245.

Dugan, B., McNeill, L.C., Petronotis, K.E., the Expedition 362 Scientists. 2017. Expedition 362 Preliminary Report: Sumatra Subduction Zone. International Ocean Discovery Program. http://dx.doi.org/10.14379/iodp.pr.362.2017

Einsele, G., Ratschbatcher, L. and Wetzel, A. 1996. The Himalaya-Bengal Fan denudation-accumulation system during the past 20 Ma. *The Journal of Geology*, **104**, 163–184.

Emmel, F.J. and Curray, J.R. 1984. The Bengal Submarine Fan, Northeastern Indian Ocean. *Geo-Marine Letters*, **3**, 119–124.

Fergusson, C.L. and Coney, P.J. 1992. Implications of a Bengal Fan-type deposit in the Paleozoic Lachlan fold belt of southeastern Australia. *Geology*, **20**, 1047–1049.

Fournier, L., Fauquembergue, K., Zaragosi, S., Zorzi, C., Malaizé, B., Bassinot, F., Joussain, R., Colin, C., Moreno, E. and Leparmentier, F. 2017. The Bengal Fan: External controls on the Holocene Active Channel turbidite activity. *The Holocene*, **27**, 900–913.

France-Lanord, C. and Derry, L.A. 1994. $\delta^{13}C$ of organic carbon in the Bengal Fan: Source evolution and transport of C3 and C4 plant carbon to marine sediments. *Geochemica et Cosmochemica Acta*, **58**, 4809–4814.

France-Lanord, C. and Derry, L.A. 1997. Organic carbon burial forcing of the carbon cycle from Himalayan erosion. *Nature*, **390**, 65–67.

France-Lanord, C., Derry, L. and Michard, A. 1993. Evolution of the Himalaya since Miocene time: isotopic and sedimentological evidence from the Bengal Fan. *In*. Treloar, P.J. and Searle, M.P. (eds). *Himalayan Tectonics*. Geological Society of London Special Publication, **74**, 603–621.

France-Lanord, C., Spiess, V., Klaus, A., Schwenk, T. and the Expedition 354 Scientists, 2016. Bengal Fan. *Proceedings of the International Ocean Discovery Program*, **354**. College Station, Teaxs (International Ocean Discovery Program). http://dx.doi.org/10.14379/iodp.proc.354.2016

Galy, V., France-Lanord, C., Beyssac, O., Faure, P., Kudrass, H. and Palhol, F. 2007. Efficient organic carbon burial in the Bengal fan sustained by the Himalayan erosional system. *Nature*, **450**, 407–410.

Geersen, J., Bull, J.M., McNeill, L.C., Henstock, T.J., Gaedicke, C., Chamot-Rooke, N. and Delescluse, M. 2015. Pervasive deformation of an oceanic plate and relationship to large >MW8 intraplate earthquakes: The northern Wharton Basin, Indian Ocean. *Geology*, **43**, 359–362.

Hall, R. 2012. Late Jurassic-Cenozoic reconstructions of the Indonesian region and the Indian Ocean. *Tectonophysics*, **570–571**, 1–41.

Haughton, P., Davis, C., McCaffrey, W. and Barker, S. 2009. Hybrid sediment gravity flow deposits – Classification, origin and significance. *Marine and Petroleum Geology*, **26**, 1900–1918.

Herman, F., Seward, D., Valla, P.G., Carter, A., Kohn, B., Willet, S.D. and Ehlers, T.A. 2013. Worldwide acceleration of mountain erosion under a cooling climate. *Nature,* **504**, 423–426

Jena B., Kurian, P.J. and Avinash, K. 2016. Morphology of submarine channel-levee systems in the eastern Bay of Bengal near Andaman region. *Journal of Coastal Conservation*, **20**, 211–220.

Joussain, R., Colin, C., Liu, Z., Meynardier, L., Fournier, L., Fauquembergue, K., Zaragosi, S., Schmidt, F., Rojas, V., Bassinot, F. 2016. Climatic control of sediment transport from the Himalayas to the proximal NE Bengal Fan during the last glacial-interglacial cycle. *Quaternary Science Reviews*, **148**, 1–16.

Jutzeler, M., White, J.D.L., Talling, P.J., McCanta, M., Morgan, S., Le Friant, A. and Ishizuka, O. 2014. Coring disturbances in IODP piston cores with implications for offshore record of

volcanic events and the Missoula megafloods. *Geochemistry, Geophysics, Geosystems*, **15**, 3572–3590.

Karig, D.E., Lawrence, M.B., Moore, G.E. and Curray, J.R. 1980. Structural framework of the forearc basin, NW Sumatra. *Journal of the Geological Society of London*, **137**, 77–91.

Lee, H., Galy, V., Feng, X., Ponton, C., Galy, A., France-Lanord, C. and Feakins, S.J., 2019. Sustained wood burial in the Bengal Fan over the last 19 My. Proceedings of the National Academy of Sciences, 1–8. https://doi.org/10.1073/pnas.1913714116

Lewis, K. 1994. The 1500-km-long Hikurangi Channel: trench-axis channel that escapes its trench, crosses a plateau and feeds a fan drift. *Geo-Marine Letters*, **14**, 19–28.

Limonta, M., Resentini, A., Carter, A., Bandopadhyay, P.C. and Garzanti, E. 2017. *In*: Bandopadhyay, P.C. and Carter, A. (eds), The Andaman–Nicobar Accretionary Ridge: Geology, Tectonics and Hazards. Geological Society, London, Memoirs, **47**, 141–152.

Manville, V. and Wilson, J.N. 2004. Vertical density currents: A review of their potential role in the deposition and interpretation of deep-sea ash layers. *Journal of the Geological Society, London*, **161**, 947–958.

McNeill, L.C., Dugan, B., Petronotis, K. 2016. Expedition 362 Scientific Prospectus: The Sumatra subduction zone. College Station, Texas (International Ocean Discovery Program). https://doi.org/10.14379/iodp.sp.362.2016.

McNeill, L.C., Dugan, B., Backman, Pickering, K.T., Pouderoux, H.F.A., Henstock, T., Petronotis, K.E., Carter, A, Chemale, F.Jr., Milliken, K.L., Kutterolf, S., Mukoyoshi, H., Chen, W., Kachovich, S., Mitchison, F.L., Bourlange, S., Colson, T.A., Frederik, M.C.G., Guèrin, G., Hamahashi, M., House, B.M., Hüpers, A., Jeppson, T.N., Kenigsberg, A.R., Kuranaga, M., Nair, N., Owari, S., Yehua, S., Song, I., Torres, M.E., Vannucchi, P., Vrolijk, P.J., Yang, T. and Zhao, X. 2017a. Understanding Himalayan erosion and significance of the Nicobar Fan. *Earth and Planetary Science Letters*, **475**, 134–142.

McNeill, L.C., Dugan, B., Petronotis, K.E. and the Expedition 362 Scientists. 2017b. Sumatra Subduction Zone. *Proceedings of the International Ocean Discovery Program,* **362**. College Station, Texas (International Ocean Discovery Program). https://doi.org/10.14379/iodp.proc.362.101.2017.

Métivier, F., Gaudemer, Y., Tapponier, P. and Klein, M. 1999. Mass accumulation rates in Asia during the Cenozoic. *Geophysical Journal International*, **137**, 280–318.

Milliman, J.D. and Syvitski, J.P.M. 1992. Geomorphic/Tectonic control of sediment discharge to the ocean: The importance of small mountainous rivers. *The Journal of Geology*, **100**, 525–544.

Moore, D.G., Curray, J.R. and Emmel, F.J. 1976. Large submarine slide (olistostrome) associated with Sunda arc subduction zone, northeast Indian Ocean. *Marine Geology*, **21**, 211–226.

Moore, D.G., Curray, J.R. and Emmel, F.J. 1982. Sedimentation in the Sunda trench and forearc region. *Geological Society, London, Special Publication*, **10**, 245–258.

Pal, T., Chakraborty, P.P., Gupta, T.D. and Singh, C.D. 2003. Geodynamic evolution of the outer-arc-forearc belt in the Andaman Islands, the central part of the Burma-Java subduction complex. *Geological Magazine*, **140**, 289–307.

Pattan, J. N., Pearce, N. J. G., Banakar, V. K. and Parthiban, G. 2002. Origin of ash in the Central Indian Ocean Basin and its implication for the volume estimate of the 74,000 year BP Youngest Toba eruption. *Current Science*, **83-7**, 889–893.

Patton, J.R., Goldfinger, C., Morey, A.E., Ikehara, K., Romsos, C., Stoner, J., Djadjadihardja, Y., Ardhyastuti, S., Gaffar, E.Z. and Vizcaino, A. 2015. A 6600 year earthquake history in the region of the 2004 Sumatra-Andaman subduction zone earthquake. *Geosphere*, **11**, 2067–2129.

Peirce, J., Weissel, J., *et al.* 1989. *Proceedings of the Ocean Drilling Program, Initial Reports,* **121**. Ocean Drilling Program, College Station Texas. http://dx.doi.org/10.2973/odp.proc.ir.121.1989.

Pickering, K.T. and Corregidor, J. 2005. Mass-transport complexes (MTCs) and tectonic control on basin-floor submarine fans, middle Eocene, South Spanish Pyrenees. *Journal of Sedimentary Research*, **75**, 761–783.

Pickering, K.T., Stow, D.A.V., Watson, M.P. and Hiscott, R.N. 1986. Deep-water facies, processes and models: a review and classification scheme for modern and ancient sediments. *Earth-Science Reviews*, **23**, 75–174.

Pickering, K.T. and Hiscott, R.N. (with contribution by Heard, T.G.) 2016. *Deep Marine Systems: Processes, Deposits, Environments, Tectonic and Sedimentation*. Wiley and American Geophysical Union (AGU), 672 pp. ISBN: 978-1-4051-2578-9.

Reading, H.G. and Richards, M. 1994. Turbidite systems in deep-water basin margins classified by grain-size and feeder system. American Association of Petroleum Geologists Bulletin, **78**, 792–-822.

Roy, T.K. 1983. Geology and hydrocarbon prospects of Andaman and Nicobar basin. *Petroleum Asia Journal*, **1**, 37–50.

RR0705 Superquakes 07 Cruise Report, 2007. Oregon State University, Active Tectonics Laboratory, United States and Agency For the Assessment and Application of Technology, Indonesia. http://www.activetectonics.coas.oregonstate.edu/sumatra/report/index.html

Schmitt, D.R., Currie, C.A. and Zhang, L. 2012. Crustal stress determination from boreholes and rock cores: Fundamental principles. *Tectonophysics*, **580**, 1–26.

Schwenk, T. and Spiess, V. 2009. Architecture and stratigraphy of the Bengal Fan as response to tectonic and climate revealed from high-resolution seismic data. *Society of Economic Paleontologists and Mineralogists Special Publication*, **92**, 107–131.

Stow, D.A.V., Amano, K., Balson, P.S., Brass, G.W., Corrigan, J., Raman, C.V., Tiercelin, J.-J., Townsend, M. and Wijayananda, N.P. 1990. Sediment facies and processes on the distal Bengal Fan, Leg 116. *In*: *Proceedings Ocean Drilling Program, Scientific Results*, **116**. Ocean Drilling Program, College Station, Texas, 377–396.

Srisuriyon, S. and Morley, C.K. 2014. Pull-apart development at overlapping fault tips: Oblique rifting of a Cenozoic continental margin, northern Mergui Basin, Andaman Sea. *Geosphere*; 10, 80–106.

Stuiver, M., Reimer, P.J. and Reimer, R.W. 2017. CALIB 7.1 [WWW program] at http://calib.org, accessed 2017-7–4.

Sumner, E.J., Siti, M.I., McNeill, L.C., Talling, P.J., Henstock, T.J., Wynn, R.B., Djajadihardja, Y.S. and Permana, H. 2013. Can turbidites be used to reconstruct a paleoearthquake record for the central Sumatran margin? *Geology*, **41**, 763–766.

Tappin, D.R., McNeill, L.C., Henstock, T. and Mosher, D.C. 2007. Mass wasting processes offshore Sumatra. *In*: Lykousis, V., Sakellariou, D. and Localt, J. (eds), *Submarine Mass Movements and Their Consequences*, 327–336. Advances in Natural and Technological Hazards Research, **47**. Dordrecht, The Netherlands: Springer.

Underwood, M.B. and Bachman, S.B. 1982. Sedimentary facies associations within subduction complexes. *Geological Society, London, Special Publication*, **10**, 537–550.

von der Borch, C.C., Sclater, J.G. *et al.* 1974. *Initial Reports Deep Sea Drilling Program*, **22**. U.S. Government Printing Office, Washington. http://dx.doi.org/10.2973/dsdp.proc.22.1974.

Weber, M.E., Wiedicke-Hombach, M., Kudrass, H.R. and Erlenkeuser, H. 2003. Bengal Fan sediment transport activity and response to climate forcing inferred from sediment physical properties. *Sedimentary Geology*, **155**, 361–381.

Yang, S-Y. and Kim, J.W. 2014. Pliocene basin-floor fan sedimentation in the Bay of Bengal (offshore northwest Myanmar). *Marine and Petroleum Geology*, **49**, 45–58.

TABLE CAPTIONS

Table 1. Biostratigraphy ages, linear sediment accumulation rates (LSAR) and mass accumulation rates (MAR) at sites U1480 and U1481. LSAR and MAR, calculated between each tie point, do not apply at depth in Site U1480.

Table 2. Raw and calibrated radiocarbon ages at Site U1480. Refer to *Supporting Information* for detailed methodology on radiocarbon age calibration.

Table 3. Classification of Nicobar Fan facies. Refer to *Supporting Information* for detailed description.

Table 4. Classification of seismic facies.

FIGURE CAPTIONS

Fig. 1. Regional map of the Bengal-Nicobar Fan System composed of the Bengal Fan, the Nicobar Fan (delineated by white long-dash line) and the 'Investigator Fan'. The map includes the deep-marine sedimentary system with fans separated by ridges, the Ganges–Brahmaputra River system, and relevant DSDP/ODP/IODP drill sites. The 'Investigator Fan', where DSDP Site 211 is located, is named after the Investigator Ridge. Discrete channels identified on the seafloor are shown (after Curray & Moore, 1971), including the Bengal Channel (BC) and Nicobar Channel (NC). The path of the NC is extrapolated (dashed lines) between observations in GoogleEarth© imagery and data from published material (bold line). Submarine channels in black are mapped on the Bengal Fan, and those in white are on the Nicobar Fan. Top right inset is a bathymetric map of the seafloor around IODP Expedition 362 sites (modified from Geersen *et al.*, 2015); note the presence of the well-identified NC continuing south of the IODP 362 sites (dashed arrows). The black box at *ca* 10°N shows the study area of Jena *et al.* (2016) who showed the connection between channel E7 in the Bengal Fan (and possibly E6) and the NC. Red dots in the enlarged seafloor image show location IODP sites U1480 and U1481. Two red lines show the position of seismic lines that include IODP sites U1480 and U1481.

Fig. 2: Simplified lithostratigraphic description of cores at Site U1480 as described in holes U1480E, U1480H, U1480F and U1480G (after McNeill *et al*., 2017a; b). These four holes are

located within a *ca* 40 m radius, each of them coring at specific depths (heavy black lines). LU: lithological units. FA: common facies associations in the interval (common FA in brackets; rare FA not mentioned). Recovery column highlights the proportion of recovered cored material (in black) in each section. See Appendix Fig. 2 for centimetre-scale description of the cores (lithology, facies, recovery, preservation and location of age samples).

Fig. 3: Simplified lithostratigraphic description of cores at Site U1481 as described in Hole U1480A (after McNeill *et al*. 2017a; b). LU: lithological units; LU in brackets at corresponding LU at Site U1480 (after McNeill *et al*.; 2017b). FA: common facies associations in the interval (common FA in brackets; rare FA not mentioned). Recovery column highlights the proportion of retrieved cored material (in black) in each section. See Appendix Fig. 2 for centimetre-scale description of the cores (lithology, facies, recovery, preservation and location of age samples).

Fig. 4: Detailed age model as defined by biostratigraphy (biostratigraphy (after McNeill *et al.*, 2017a and Backman *pers. com.* 2017, but see Backman *et al*., 2019 for modified ages) and radiocarbon dating (this study). Tie points are presented in Table 1. Roman numbers represent lithological units defined in McNeill *et al.* (2017b). Red and orange dots are biostratigraphy tie points in sites U1480 and U1481. Between each tie point, the linear sediment accumulation rate (LSAR in m Myr^{-1}) is given. The central inset show an expanded view of the Pleistocene Period, and the right inset shows radiocarbon ages (^{14}C data; green dots) collected in the upper 2 m at Site U1480. The oldest radiocarbon age at *ca* 50 ka is not consider reliable as it is at the time limit of the radiocarbon dating technique. Younger ages show a stable 20 m Myr^{-1} LSAR, which suggests the tephra bed identified at *ca* 1.8 m in Site U1480 (Appendix Fig. 3) is the Young Toba Tephra (YTT) dated at 74 ka (Pattan *et al.*, 2002).

Fig. 5: Photographs of facies identified in Holes U1480 and U1481. All photographs are at the same vertical scale and horizontal scale. Arrows indicate the boundary between facies, and in the case of SGF deposits, the base of the bed. (**A**) Core U1480H-11H, section 2, 40 to 73 cm. (**B**) Core U1480H-2H, section 4, 53 to 78 cm. (**C**) Core U1480F-96X, section 2, 0 to 50 cm. (**D**) Core U1481A-30R, section 6, 42 to 82 cm. (**E**) Core U1481A-21R, section 1, 30 to 82 cm. (**F**) Core U1480E-1H, section 1, 16 to 42 cm. (**G**) U1480G-69R, section 7, 25 to 55 cm. (**H**)

Core 1480G-62R, section 4, 85 to 118 cm. (**I**) Core U1480H-2H, section 5, 100 to 124 cm. (**J**) Core U1480H-2H, section 3, 64 to 79 cm. (**K**) Core U1480F-26F, section 1, 35 to 70 cm. (**L**) Core U1480E-11H, section 1, 30 to 60 cm. (**M**) Core U1480G-14R, section 3, 52 to 76 cm. (**N**) Core U1480G-54R, section 1, 40 to 70 cm. (**O**) Core U1480F-78X, section 1, 30 to 50 cm. (**P**) Core U1480G-69R, section 8, 10 to 35 cm. (**Q**) Core U1480G-61R, section 4, 24 to 57 cm.

Fig. 6: Regional cross-section showing the seismic architecture (top) and seismic stratigraphy (bottom) of the Nicobar Fan at *ca* 3°N (see Fig. 1 for location). Uninterpreted seismic profiles BRG06-102/101 are extracted from Geersen *et al.* (2015) and McNeill *et al.* (2017b). The exact location of Site U1480 is shown (bold black line), as well as the major seismic unit presented in the text (SU1 to SU4). Subvertical black lines represents faults, and subhorizontal coloured lines are major seismic reflectors labelled R1 to R14 from top to base. Divisions in the bottom seismic stratigraphic interpretation are explained in Fig. 7. NC: Nicobar Channel (see Fig. 1).

Fig. 7: Core-seismic integration at Site U1480. Seismic reflectors (coloured crosses) are those picked in Fig. 6. The age of the reflectors is estimated by the time-depth conversion applied by McNeill *et al.* (2017b) and a linear sedimentation rate deduced from the age model presented in Fig. 4. Numbers (1 to 19) in the depth-age plot correspond to tie points (see Table 1). Note that the tie point ages are approximate and the ages assigned to the reflectors using constant sedimentation rates between them are also estimated. Note also that the reflectors are not necessarily correlated to lithostratigraphic unit boundaries, although some can be used as proxy of main time markers. R5, dated at *ca* 2.7 Ma, is a good proxy for the base of the Pleistocene (i.e. 2.58 Ma; GTS2012). R7, dated at *ca* 5.8 Ma, is a good proxy for the base of the Pliocene (i.e. 5.33 Ma; GTS2012). R11 and R12, dated at *ca* 10 Ma and *ca* 17.5 Ma, serve as proxies for the base of the late Miocene and middle Miocene, respectively.

Fig. 8: Close up of Fig. 6 in the vicinity of Site U1480 showing reflector interpretations (top; after McNeill *et al.*, 2017b) and seismic facies interpretations (bottom). Top image shows the coloured seismic reflectors R1 to R14 and the location of Site U1480 holes. The depth scale on the right accounts for the time-depth conversion presented in Fig. 7. Bottom image presents the different seismic facies (S1 to S5) identified in this study. The thin units of

hemipelagites at 0 to 6 mbsf and *ca* 18 to 25 mbsf (LU-IA and LU-IC) are below seismic resolution; in higher resolution, these units may appear as Seismic Facies S3. Bold dashed lines represent lithological unit boundaries (LU-x). EOC: End of Core. S_0-1, S_0-2 and S_0-3 refer to the type of channels described in Table 4.

Fig. 9: Summary of mass accumulation rates (MAR in $g{\cdot}cm^{-2}{\cdot}kyr^{-1}$) in the Bengal-Nicobar Fan System, represented by Site U1453 (purple) on the Ninetyeast Ridge, Site U1451 (green) in the Bengal Fan and sites U1480 (red) and U1481 (yellow) in the Nicobar Fan (Fig. 1 for location). The MAR are reported in Table 1 (U1480 and U1481) and in Appendix Tables 4 and 5 for other sites. Colours in the stratigraphic scale are those used in seismic stratigraphy figures (Figs 6, 7 and 11). The dominant sedimentary processes as deduced from core analyses are shown for each site: either SGFs (yellow horizontal double arrows) or hemipelagic sedimentation (blue horizontal double arrows). The *ca* 40.7 Myr long hiatus (58.1 to 17.4 Ma) in Site U1480 as well as the possible one (or condensed section) proposed at *ca* 15 to 18 Ma are shown. For the Bengal Fan, the MAR values that were calculated for Site U1451 (plain lines) are shown, as well as the maximum MAR (dashed lines) estimated using the observations of Shwenk & Spiess (2009) that sediment accumulation rates at Site U1451 were *ca* 75% of the maximum values for the Late Miocene (10 to 5.33 Ma), *ca* 40% for the Pliocene (5.33 to 1.8 Ma) and *ca* 30% for the Pleistocene (1.8 to 0 Ma).

Fig. 10: Close-up view of the Eocene–Oligocene hiatus in Site U1480 (biostratigraphically placed at 1326.39 ± 0.43 mbsf 1326.71 mbsf; core U1480G-61R-7A). The subhorizontal, highly bioturbated surface at 1326.71 mbsf (section U1480G-61R-7A 45 cm) interpreted as a hard ground surface is likely associated to that hiatus.

Fig. 11: Seismic stratigraphy of the Bengal Fan (line GeoB97-020/027) and the Nicobar Fan (BRG06-102/101). See Fig. 1 for location. The definition of stratigraphic units is detailed in Appendix Fig. 4. Interpretation of seismic line GeoB97-020/027 is from Schwenk & Spiess (2009), updated by France-Lanord *et al.* (2016), according to the revised age model of McNeill *et al.* (2017b) of Site U1451 (see Appendix Fig. 4). Dashed lines in GeoB97-020/027 are unconformities identified by Schwenk & Spiess (2009); the top one is the Pleistocene unconformity, the bottom one in the Pliocene unconformity. Interpretation of seismic line BGR06-102/101 is detailed in Fig. 6.

Fig. 12. Seismic images of Nicobar Fan channel-type examples. Vertical exaggeration = x5. Faults and horizons are not interpreted. (**A**) Seafloor compound channel (pale yellow line outlining channel base; other channels also interpreted) Note the candidate lateral accretion packages dipping to right. (**B**) Compound channel example (green line outlining channel base, yellow lines outlining small channels within). (**C**) Simple channel example, triangle-shape (green line outlining channel base; other channels also interpreted). (**D**) Simple channel example, ellipse-shape (green line outlining channel base).

Fig. 13. Nicobar Fan channel shape and size data. (**A**) Channel width:depth for both compound and simple channels. (**B**) Channel area with depth for all channels interpreted, with stratigraphic units and subunits from IODP Site U1480 and channel type (compound versus simple) indicated. (**C**) Frequency distribution of channel width:depth ratios with best-fit Weibull curve overlain (red line). (**D**) Channel frequency with depth and stratigraphic units and subunits from IODP Site U1480. For data table used to create these graphs, see Appendix Table 7.

Fig. 14: Palaeogeographic reconstructions of the Bengal-Nicobar Fan System (BNFS), modified from McNeill *et al.* (2017a). Tectonic reconstruction used is from Hall (2012). Bengal Fan morphology from Curray (2014); core data from DSDP/ODP/IODP sites (white dots; red dots = IODP Expedition 362 sites). In this paper, sediment mass accumulation rates (MAR) were calculated for Sites U1451 (green dot), U1453 (purple dot) and U1480-1481 (red dots; see Fig. 9): the white dots are other drill DSDP/ODP/IODP sites. The postulated earliest submarine-fan deposits are shown as routing along the eastern side of the Indian Ocean, as axial SGFs along the Sunda subduction zone trench until it was overfilled to construct the Bengal Fan. The latest Eocene and early Oligocene Andaman Flysch, now as accreted and uplifted sedimentary rocks forming part of the Andaman Islands, is the oldest interpreted trench deposits (*ca* 30 Ma map). Also, note the much increased coarser-grained terrigenous sediment supply to the Bengal Fan between 13.5 to 8.5 Ma (but beginning at *ca* 27 Ma), switching to the Nicobar Fan after *ca* 9.5 to 9.0 Ma, and then back to the Bengal Fan after *ca* 2 Ma (see Fig. 9).

Appendices Supplementary Material

Appendix Figure 1: Age model of DSDP Leg 22 Site 211 calibrated during IODP Expedition 362 after von der Borch *et al*. (1974).

Appendix Figure 2: Core description with facies (using scheme of Pickering *et al*. (1986), updated in Pickering and Hiscott (2016) for Hole. U1481.

Appendix Figure 3: Comparative sections of the same stratigraphic interval *ca* 50 m apart (*ca* 70 to *ca* 90 mbsf) drilled in sites U1480E and U1480H. See Fig. 2 for legend. Despite excellent core recovery of 100 to 109% (>100% due to core expansion with retrieval), the sedimentary column is incomplete as recovered material is strongly deformed by coring procedures. Although the upper part of the core is relatively well preserved (red and purple intervals), significant portions of the column are missing towards the base of cores, and particularly in Hole H. For example, core U1480H-9H is missing the blue and orange intervals, characterized by a strong change in sedimentary dynamics. This example means that caution is necessary encourages when interpreting highly deformed cored intervals (moderate to severe drilling disturbance using the terminology of this study) in term of facies thickness and sedimentary processes.

Appendix Figure 4: Regional cross section showing the seismic architecture of the Nicobar Fan at *ca* 3°N (Fig. 1 for location). Uninterpreted seismic profiles BRG06-102/101 are from Geersen *et al*. (2015) and McNeill *et al*. (2017b). The precise location of Site U1481 is shown (bold black line). Subvertical black line represents faults, and subhorizontal coloured lines are the major seismic reflectors, R1 to R14, that are correlated in Fig. 6. NC: Nicobar Channel (see Fig. 1).

Appendix Figure 5: Core-seismic integration at Site U1451 (**A**) and U1480 (**B**). The age model (red curve) is plotted after the updated ages of McNeill *et al*. (2017a) for both sites. The time-depth conversion (blue curve) is plotted after IODP Expedition reports (France-Lanord *et al*., 2016; McNeill *et al*., 2017b). Seismic reflectors (coloured crosses) represent time markers used in seismic stratigraphy (Figs 6 and 11) and are different from the reflectors R1 to R14.

Appendix Table 1: Updated biostratigraphy ages of DSDP Leg 22 Site 211.

Appendix Table 2: Types of coring disturbance observed at IODP Expedition 362 drill sites.

Appendix Table 3: Tie points, depth (m), age (Ma), LSAR (m Myr^{-1}) and MAR (g cm^{-2} kyr^{-1}) for U1443. Compiled from McNeill *et al*. (2017a). LSAR = linear sediment accumulation rate; MAR = mass accumulation rate.

Appendix Table 4: Tie points, depth (m), age (Ma), LSAR (m Myr^{-1}) and MAR (g cm^{-2} kyr^{-1}) for U1451. Compiled from McNeill *et al*. (2017a). LSAR = linear sediment accumulation rate; MAR = mass accumulation rate.

Appendix Table 5: Tie points, depth (m), age (Ma), LSAR (m Myr^{-1}) and MAR (g cm^{-2} kyr^{-1}) for U1443. Compiled from McNeill *et al*. (2017a). LSAR = linear sediment accumulation rate; MAR = mass accumulation rate.

Appendix Table 6: Biostratigraphic tie points, lithologic unit/subunit, LSAR (m Myr^{-1}), LSAR (cm kyr^{-1}), grain density (g cm^{-3}), porosity (%), and MAR (g cm^{-2} kyr^{-1}) at Site U1480. Site U1481, Site U1451, Site U1443. LSAR = linear sediment accumulation rate; MAR = mass accumulation rate.

Appendix Table 7: Submarine channel data from two seismic profiles BGR06-101-102 (see Fig. 6) and BGR06-103-104. Data are plotted in Fig. 13.

Table 1.

Site	Tie point number	Depth (mbsf)		Age (Ma)		LSAR (m/Myr)	MAR (g/cm^2/kyr)
		Mean	Δ	Mean	Δ		
Deduced from ^{14}C		5.60		0.280		20	1.3
U1480	1	18.17	0.61	0.430		78	8.0
U1480	2	19.47		0.850		3	0.2
U1480	3	24.13		1.120	0.100	17	1.4
U1480	4	27.07		1.655	0.055	5	0.4
U1480	5	80.57		2.045	0.115	137	20.6
U1480	6	205.63	21.47	2.390		362	53.2
U1480	7	385.01	4.19	3.820		125	19.9
U1480	8	475.13		5.200	0.160	65	10.2
U1480	9	795.91		7.170	0.230	163	28.3
U1480	10	1044.86	7.63	8.315	0.115	217	40.0
U1480	11	1255.15		9.260	0.750	223	43.0
U1480	12	1269.16		10.200	0.420	15	2.9
U1480	13	1313.97		18.350	0.650	5	0.9
U1480	14	1325.95		22.400		3	0.5
U1480			*HIATUS*				
U1480	15	1327.03	0.20	58.100	0.900		
U1480	16	1357.43		59.600			
U1480	17	1399.23		63.900			
U1480	*17bis*	1401.01		65.530			
U1480			*HIATUS*				
U1480	*17ter*	1401.01		66.820			
U1480	18	1401.45		66.950			
U1480	19	1407.64		68.730			
U1481	1	1159.63	5.27	8.245	0.045		
U1481	2	1370.05		9.260	0.750	207	40.0
U1481	3	1409.61	1.80	10.735	1.865	27	5.3
U1481	4	1495.97	0.44	18.805	0.115	11	2.2

Compiled from McNeill *et al*. (2017a, b, c) and Backman *pers. com*. (2017).
LSAR = linear sediment accumulation rate. MAR = Mass accumulation rate.

Table 2.

Site	Hole	Depth (mbsf)	Raw age (a) Mean	Δ	Calibrated age (a BP) Mean	Δ
U1480	E	0.17	10690	25	12079.5	366.5
U1480	E	0.87	42020	620	44976.0	1136.0
U1480	E	24.13	45370	950	48250.5	1749.5
U1480	H	0.25	12825	35	14544.5	418.5
U1480	H	0.68	30120	150	33794.0	350.0
U1480	H	1.18	44190	810	47169.0	1733.0

Table 3.

Lithological description			Facies association		Sedimentary processes
Class	**Group**	**Facies**			
B – Sands	B1 – Disorganized sands	B1.1 – Thick to medium-bedded disorganized sand	**FA8**	*Coring-induced artefacts*	*Severe coring disturbance of SGF deposits*
	B2 – Organized sands	B2.1 – Parallel-stratified sand			
C – Sand–mud couplets	C1 – Disorganized sand-mud couplets	C1.1 – Poorly sorted muddy sand	**FA3**	Candidate hybrid event beds	Candidate hybrid SGFs (possibly including concentrated density flows)
	C2 -Organized sand-mud couplets	C2.1 – Very thick to thick beds C2.2 – Medium beds C2.3 – Thin beds	**FA1a**	Sandy turbidites	Turbidity currents (possibly including concentrated density flows)
D – Silts, silty-clays and silt–clay couplets	D1 – Disorganized silts	D1.1 – Structreless silt	**FA8**	*Coring-induced artefacts*	*Severe coring disturbance of SGF deposits*
		D1.2 – Graded, poorly sorted silt	**FA3**	Candidate hybrid event beds	Candidate hybrid SGFs
	D2 – Organized silts	D2.1 – Graded-stratified silt	**FA1a**	Sandy turbidites	Turbidity currents
		D2.2 – Graded-stratified silty-clay	**FA2**	Muddy turbidites	Low-concentration turbidity currents
		D2.3 – Very thin silty-clay couplets and silt and clay laminae	**FA1a**	Sandy turbidites	Turbidity currents
E – Muds	E1 – Disorganized muds	E1.1 – Structureless mud	**FA4**	Hemipelagites	Low-concentration turbidity currents and open-ocean suspension settling
		E1.2 – Varicoloured mud	**FA5**	Pelagites	Open-ocean suspension settling
		E1.4 – Brecciated mud	**FA3**	Candidate hybrid event beds	Candidate hybrid SGFs
	E2 – Organized muds	E2.1 – Graded mud	**FA2**	Muddy turbidites	Low-concentration turbidity currents
G – Biogenic sediments	G1 – Oozes	G1.1 – Calcareous ooze	**FA5**	Pelagites	Open-ocean marine sedimentation
	G2 – Biogenic muds	G2.1 – Biogenic structureless mud	**FA4**	Hemipelagites	Open-ocean suspension settling
		G2.2 – Biogenic varicoloured mud	**FA5**	Pelagites	Open-ocean suspension settling
	G3 – Organized biogenic sediments	G3.1 – Graded biogenic mud	**FA1b**	Calcareous turbidites	Candidate hybrid SGFs
H – Pyroclastic deposits and igneous rocks	H1 – Organized pyroclastic sands and silts	H1.1 – Graded pyroclastic sand and silt	**FA6**	Airfall tephra	Vertical density current associated with subaerial volcanic eruption
	H2 – Disorganized pyroclastic gravels and	H2.1 – Volcaniclastic conglomerate	**FA7a**	Volcanic products	Subaqueous volcanic eruption
	H3 – Lava flows	H3.1 – Basaltic extrusion	**FA7a**	Volcanic products	Subaqueous lava flow
		H3.2 – Basaltic intrusion	**FA7b**	Volcanic products	Sill or dyke

Table 4

S0 – Channels	
Description:	V–U-shaped architectural elements with well-defined basal surface that truncates underlying reflectors; variable seismic character with chaotic, planar laminated or transparent reflections that are generally of average frequency and amplitude:
	S0-1 – continuous and parallel internal reflectors
	S0-2 – discontinuous and parallel internal reflectors truncated by subvertical delineations
	S0-3 – smaller than the type 2 channels, with homogeneous to transparent seismic character
Core correlation:	Rare core examples:
	S0-1 – no samples
	S0-2 – sampled at 650–740 mbsf; recovered material consistent with a highly sand-prone interval and coarse-grained SGF deposits
	S0-3 – sampled at 210 to 225 and 320 to 340 mbsf; recovered material suggesting sandy material and coarse-grained SGF deposits
Interpretation:	Deep-sea channels:
	S0-1 – aggrading pattern
	S0-2 – lateral accretion processes
	S0-3 – single-filled, isolated short-lived sedimentary structures
S1 – Lobes and lobe complexes	
Description:	Lenticular bedding composed of subparallel and laterally discontinuous reflectors with well-defined onlap and toplap terminations. Reflectors are commonly of average frequency and low to average amplitude
Core correlation:	Facies sampled three times at Site U1480 (150 to 180, 375 to 525 and 875 to 1240 mbsf). Recovered material comprises sand-rich turbidites, mud-rich turbidites, candidate hybrid event beds and hemipelagites with a crude fining upward trend locally
Interpretation:	Lobe complexes, in the absence of associated channels (S0-1 or S0-2)
S2 – Channel-levée systems and/or lobes	
Description:	Association of lenticular bedding and channels; reflectors are commonly subparallel and continuous, of average frequency and of low to average amplitude; the termination of reflectors is suggested by the progressive decreasing bed thickness but not always visible on seismic
Core correlation:	Facies sampled at 0 to 70, 90 to 125, 250 to 320, 525 to 650 and *ca* 40 to 780 mbsf; recovered material dominated by mud-rich turbidites, with rare interbedded sand-rich SGF deposits, including turbidites or candidate hybrid event beds

Interpretation:	Large channel-levée complexes and/or (associated) lobes
S3 – Inter-lobe, inter-channel and fan-fringe deposits	
Description:	Parallel and continuous reflectors characterized by average frequency and average to high amplitude
Core correlation:	Facies sampled as thin units (one reflector thick) at 80, 135, 200, 230 and 360 mbsf, and as thick units at 780 to 875 and 1240 to 1310 mbsf; thickness tends to decrease upward
	Thin units – mud-rich turbidites (<2 m thick) trapped within thick stacks of sand-rich SGF deposits including turbidites; the lithology contrast explaining the presence of reflectors
	Thick units – mud-rich turbidites and hemipelagites with rare, disseminated sand-rich turbidites and candidate hybrid event beds
Interpretation:	Hemipelagites and/or fan-fringe deposits
S4 – Pre-fan deposits	
Description:	Parallel and continuous reflectors with high frequency and low amplitude, identified directly above the acoustic basement (Seismic Facies S5)
Core correlation:	Correlated to pre-fan lithological units (LU-IIIB to LU-IV), sampled at Site U1480 at 1310 to 1360 mbsf. Those depths are characterized by stacked pelagites and calcareous SGF deposits (for example, turbidites) and extrusive volcanic deposits (including volcaniclastics)
Interpretation:	Deep-marine pelagites and volcanic deposits, that lack terrigeneous SGF deposits
S5 – Basement	
Description:	Discontinuous and disorganised reflectors of varying frequency and amplitude; Occurrence of mound-shaped structures characterized by subvertical reflectors of low frequency and average amplitude
Core correlation:	Facies boundary correlated to the top of the intrusive volcanic material (LU-V; 1360 mbsf), while the oceanic crust (LU-VI) is recognized at *ca* 1415 mbsf
Interpretation:	Acoustic basement that slightly differs from the oceanic crust *sensu stricto*; mount-shaped structures interpreted as submarine volcanoes (seamounts and ridges)

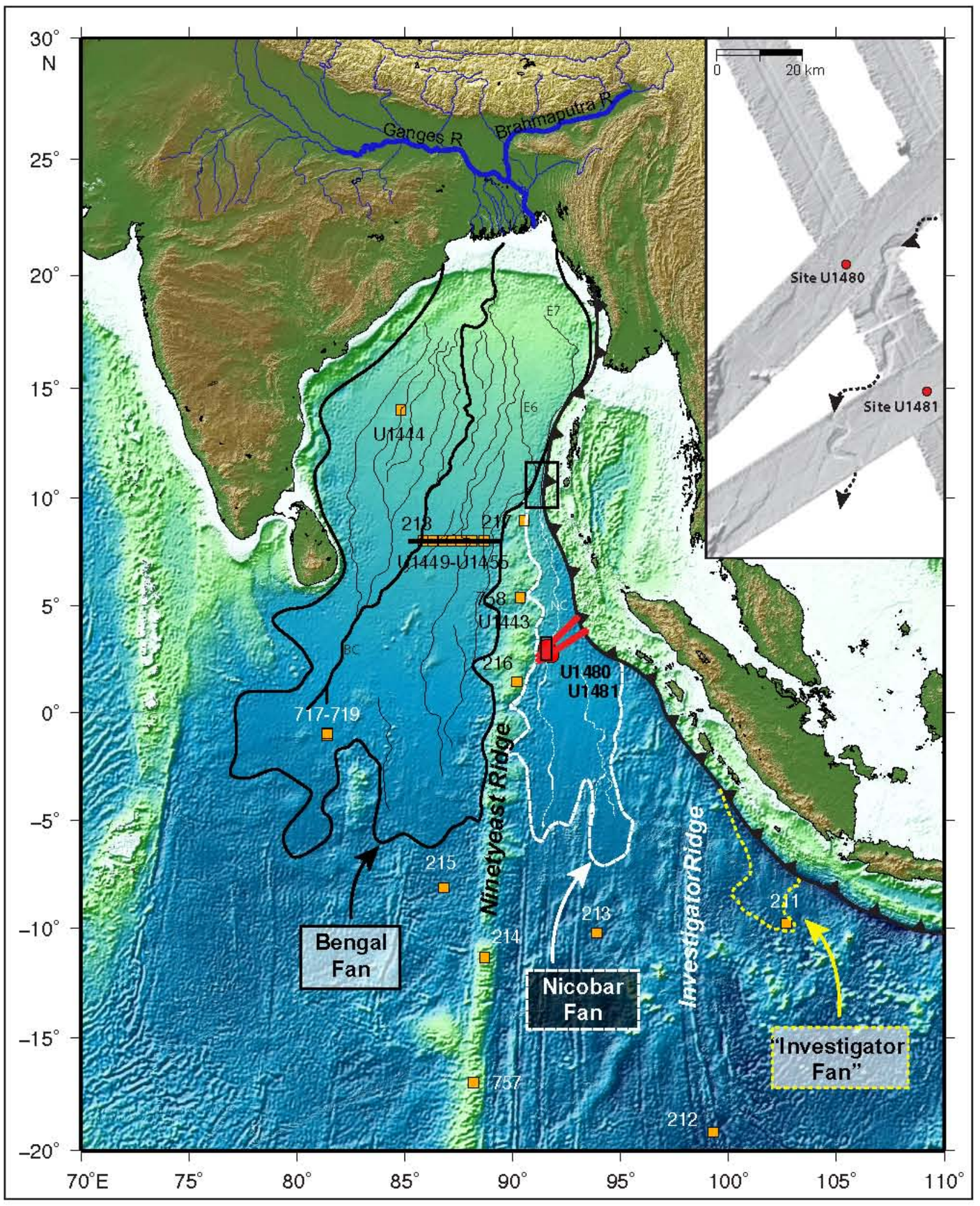
30° N
25°
20°
15°
10°
5°
0°
–5°
–10°
–15°
–20°
70°E
75°
80°
85°
90°
95°
100°
105°
110°
Ganges R
Brahmaputra R
0
20 km
Site U1480
Site U1481
E7
E6
U1444
213
217
U1449-U1456
758
U1443
NC
BC
216
U1480
U1481
717-719
215
Ninetyeast Ridge
214
213
Investigator Ridge
211
212
757
Bengal Fan
Nicobar Fan
"Investigator Fan"

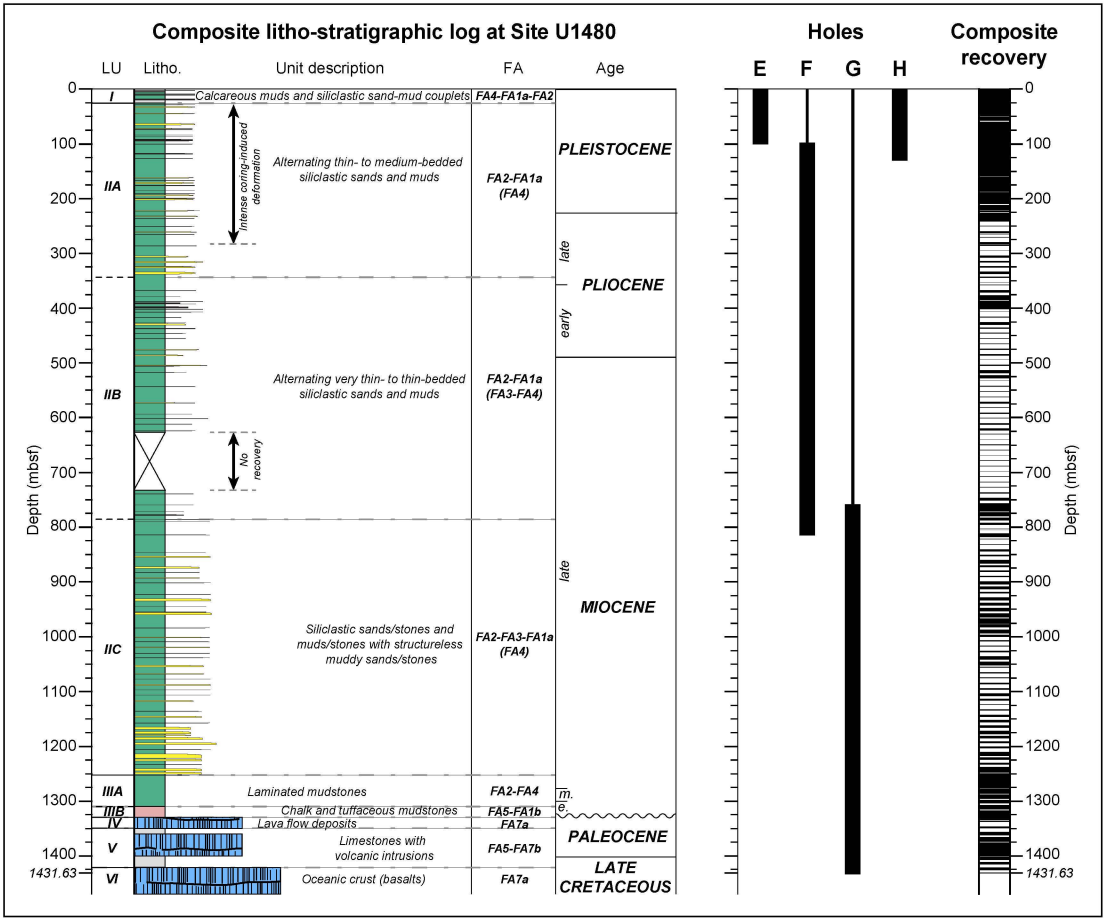
Composite litho-stratigraphic log at Site U1480
LU
Litho.
Unit description
FA
Age
Depth (mbsf)
I
IIA
IIB
IIC
IIIA
IIIB
IV
V
VI
1431.63
Calcareous muds and siliclastic sand-mud couplets
FA4-FA1a-FA2
Intense coring-induced deformation
Alternating thin- to medium-bedded siliclastic sands and muds
FA2-FA1a (FA4)
Alternating very thin- to thin-bedded siliclastic sands and muds
FA2-FA1a (FA3-FA4)
No recovery
Siliclastic sands/stones and muds/stones with structureless muddy sands/stones
FA2-FA3-FA1a (FA4)
Laminated mudstones
FA2-FA4
Chalk and tuffaceous mudstones
FA5-FA1b
Lava flow deposits
FA7a
Limestones with volcanic intrusions
FA5-FA7b
Oceanic crust (basalts)
FA7a
PLEISTOCENE
late
PLIOCENE
early
late
MIOCENE
m.
e.
PALEOCENE
LATE CRETACEOUS
Holes
E
F
G
H
Composite recovery
Depth (mbsf)

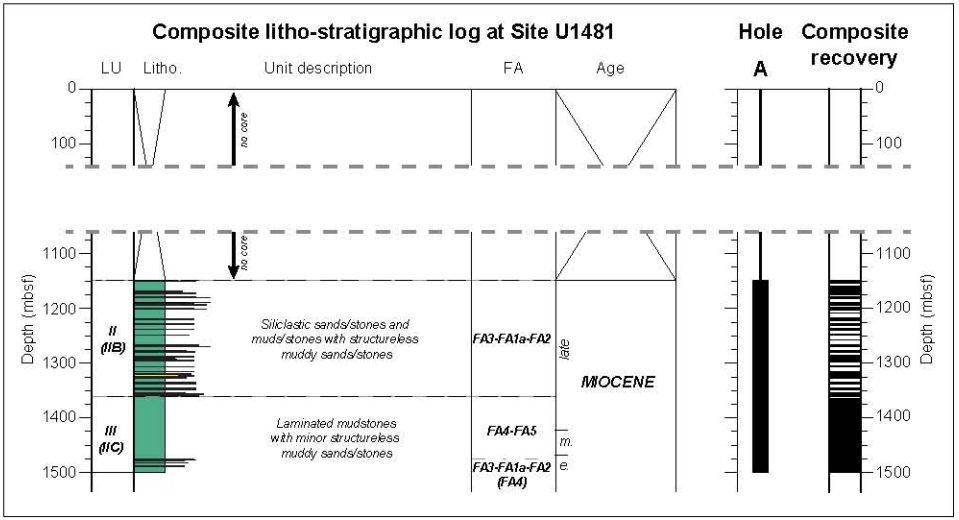
Composite litho-stratigraphic log at Site U1481
LU
Litho.
Unit description
FA
Age
Hole A
Composite recovery
0
100
no core
1100
1200
1300
1400
1500
Depth (mbsf)
II (IIB)
III (IIC)
Siliclastic sands/stones and muds/stones with structureless muddy sands/stones
Laminated mudstones with minor structureless muddy sands/stones
FA3-FA1a-FA2
FA4-FA5
FA3-FA1a-FA2 (FA4)
late
m.
e.
MIOCENE

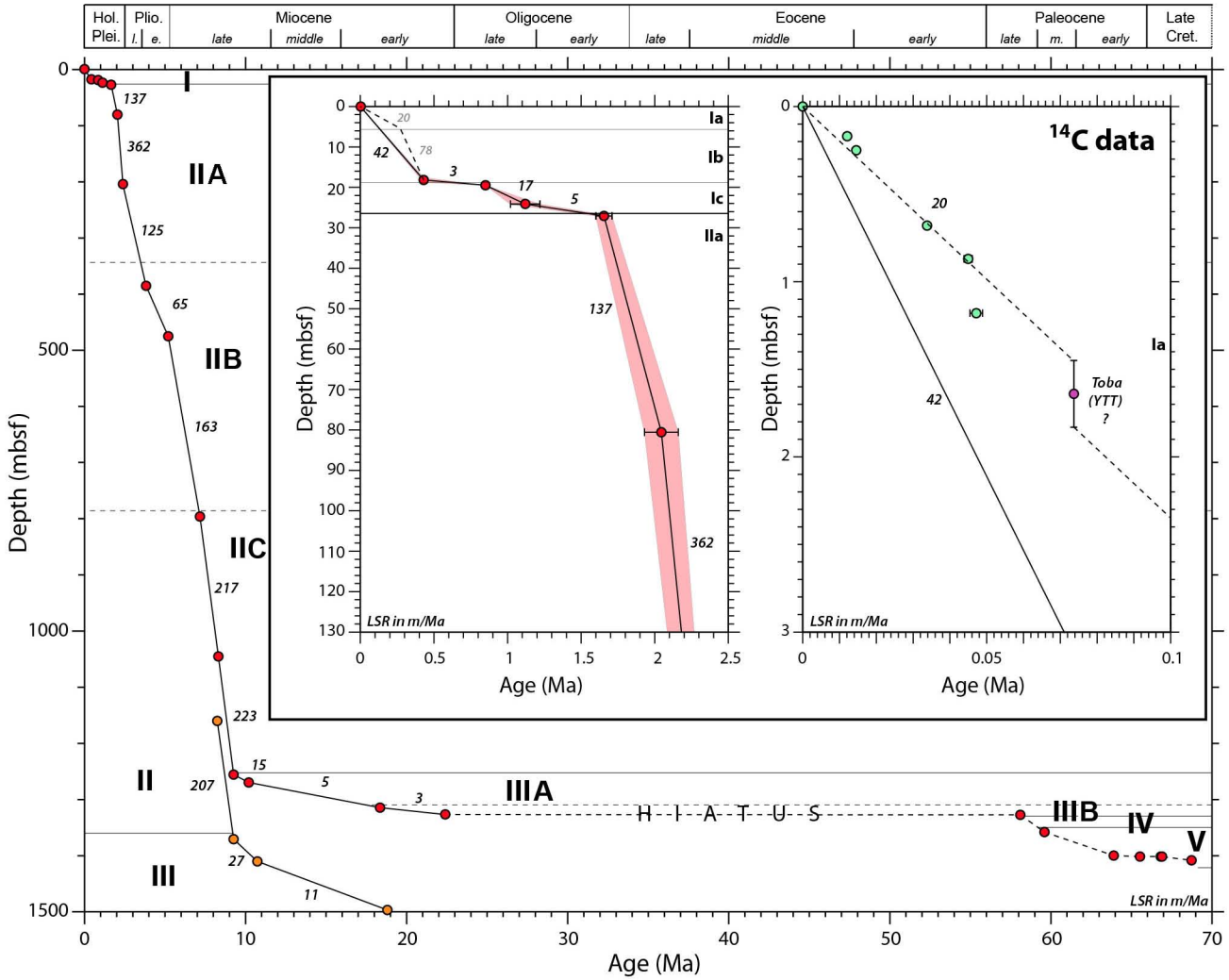
Hol.
Plei.
Plio.
l.
e.
Miocene
late
middle
early
Oligocene
late
early
Eocene
late
middle
early
Paleocene
late
m.
early
Late
Cret.
Depth (mbsf)
Age (Ma)
LSR in m/Ma
I
IIA
IIB
IIC
II
III
IIIA
H I A T U S
IIIB
IV
V
137
362
125
65
163
217
223
15
207
5
3
27
11
Ia
Ib
Ic
IIa
20
78
42
3
17
5
137
362
14C data
20
42
Toba
(YTT)
?

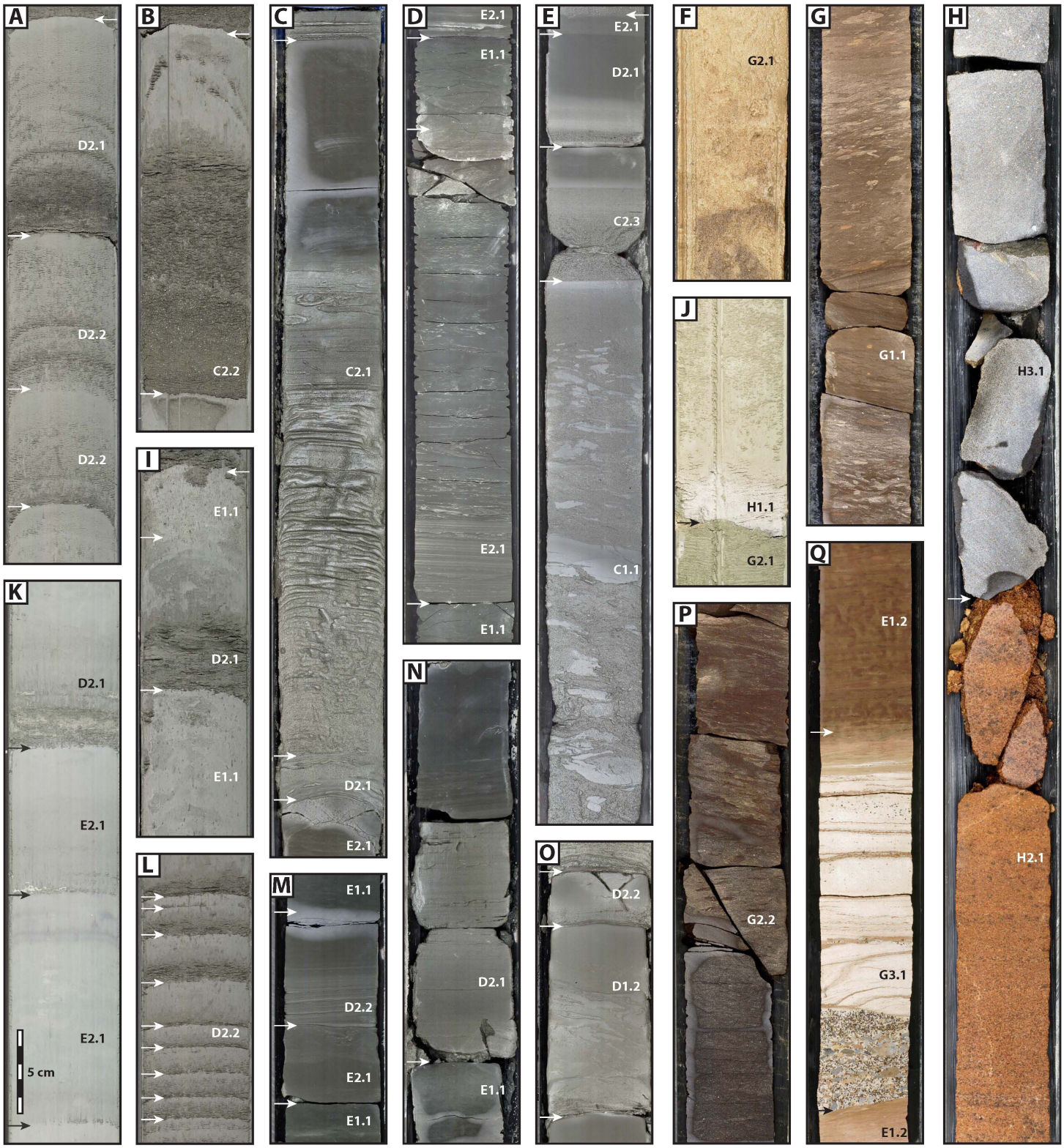
A
D2.1
D2.2
D2.2
B
C2.2
C
C2.1
D2.1
E2.1
D
E2.1
E1.1
E2.1
E1.1
E
E2.1
D2.1
C2.3
C1.1
F
G2.1
G
G1.1
H
H3.1
H2.1
I
E1.1
D2.1
E1.1
J
H1.1
G2.1
K
D2.1
E2.1
E2.1
5 cm
L
D2.2
M
E1.1
D2.2
E2.1
E1.1
N
D2.1
E1.1
O
D2.2
D1.2
P
G2.2
Q
E1.2
G3.1
E1.2

0 km 50 100 150 200 250 300 km

5.0 6.0 7.0 8.0 9.0 TWT (s)

SW

Site U1480

BRG06-102

NC

BRG06-101

NE

Subduction front

R1 R2 R3 R4 R5 R6 R7 R8 R9 R10 R11 R12 R13 R14

SU1 SU2 SU3 SU4

Acoustic basement

Ninetyeast Ridge (eastern flank)

Channel

Undetermined NER

Pleistocene

Pliocene

late Miocene

middle Miocene

Paleocene - early Miocene

Acoustic basement

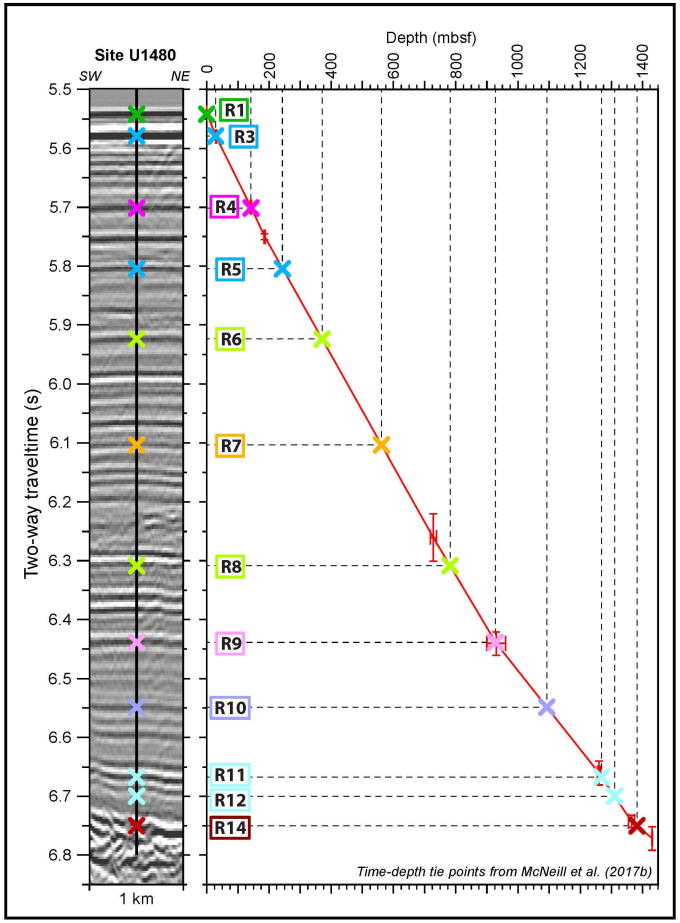
Site U1480
SW
NE
Depth (mbsf)
0
200
400
600
800
1000
1200
1400
Two-way traveltime (s)
5.5
5.6
5.7
5.8
5.9
6.0
6.1
6.2
6.3
6.4
6.5
6.6
6.7
6.8
R1
R3
R4
R5
R6
R7
R8
R9
R10
R11
R12
R14
1 km
Time-depth tie points from McNeill et al. (2017b)

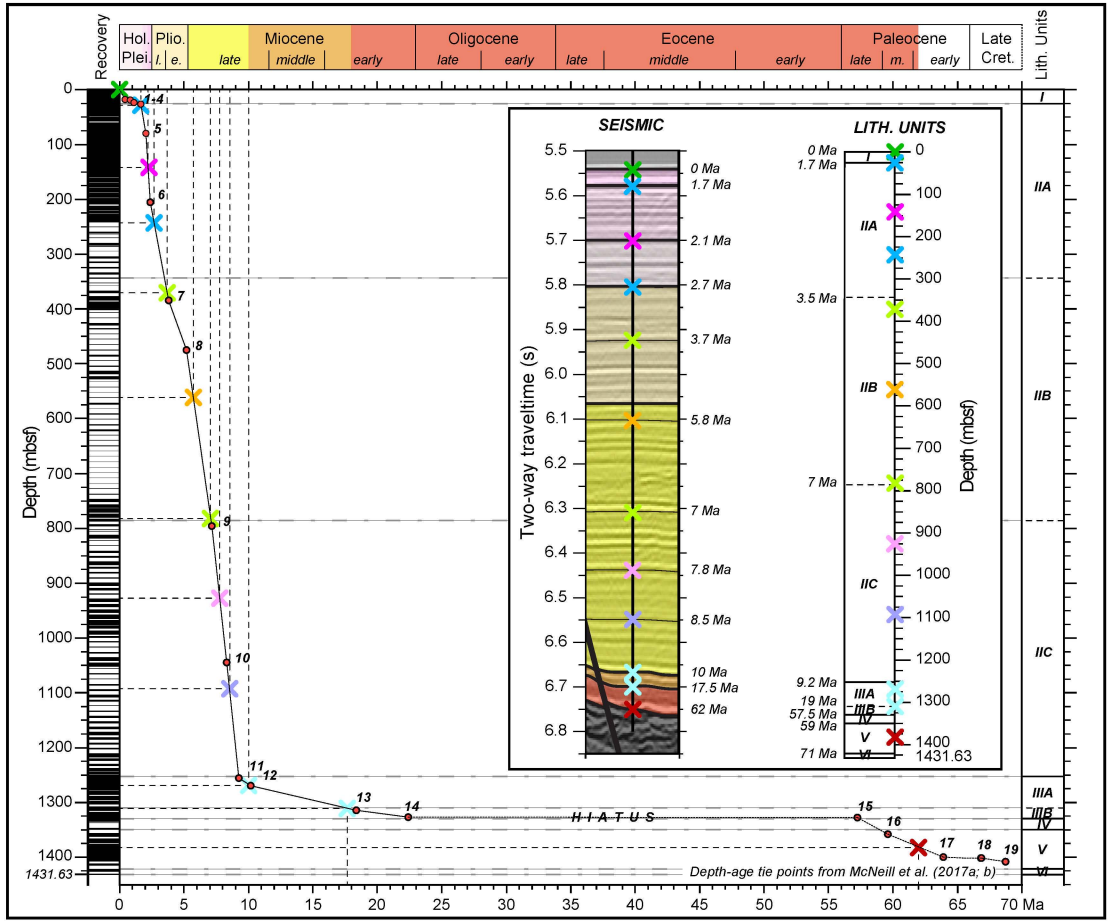
Recovery
Hol.
Plei.
Plio.
l.
e.
Miocene
late
middle
early
Oligocene
late
early
Eocene
late
middle
early
Paleocene
late
m.
early
Late
Cret.
Lith. Units
Depth (mbsf)
0
100
200
300
400
500
600
700
800
900
1000
1100
1200
1300
1400
1431.63
1 4
5
6
7
8
9
10
11
12
13
14
15
16
17
18
19
H I A T U S
0
5
10
15
20
25
30
35
40
45
50
55
60
65
70 Ma
Depth-age tie points from McNeill et al. (2017a; b)
SEISMIC
Two-way traveltime (s)
5.5
5.6
5.7
5.8
5.9
6.0
6.1
6.2
6.3
6.4
6.5
6.6
6.7
6.8
0 Ma
1.7 Ma
2.1 Ma
2.7 Ma
3.7 Ma
5.8 Ma
7 Ma
7.8 Ma
8.5 Ma
10 Ma
17.5 Ma
62 Ma
LITH. UNITS
Depth (mbsf)
0 Ma
1.7 Ma
3.5 Ma
7 Ma
9.2 Ma
19 Ma
57.5 Ma
59 Ma
71 Ma
I
IIA
IIB
IIC
IIIA
IIIB
IV
V
VI
1431.63

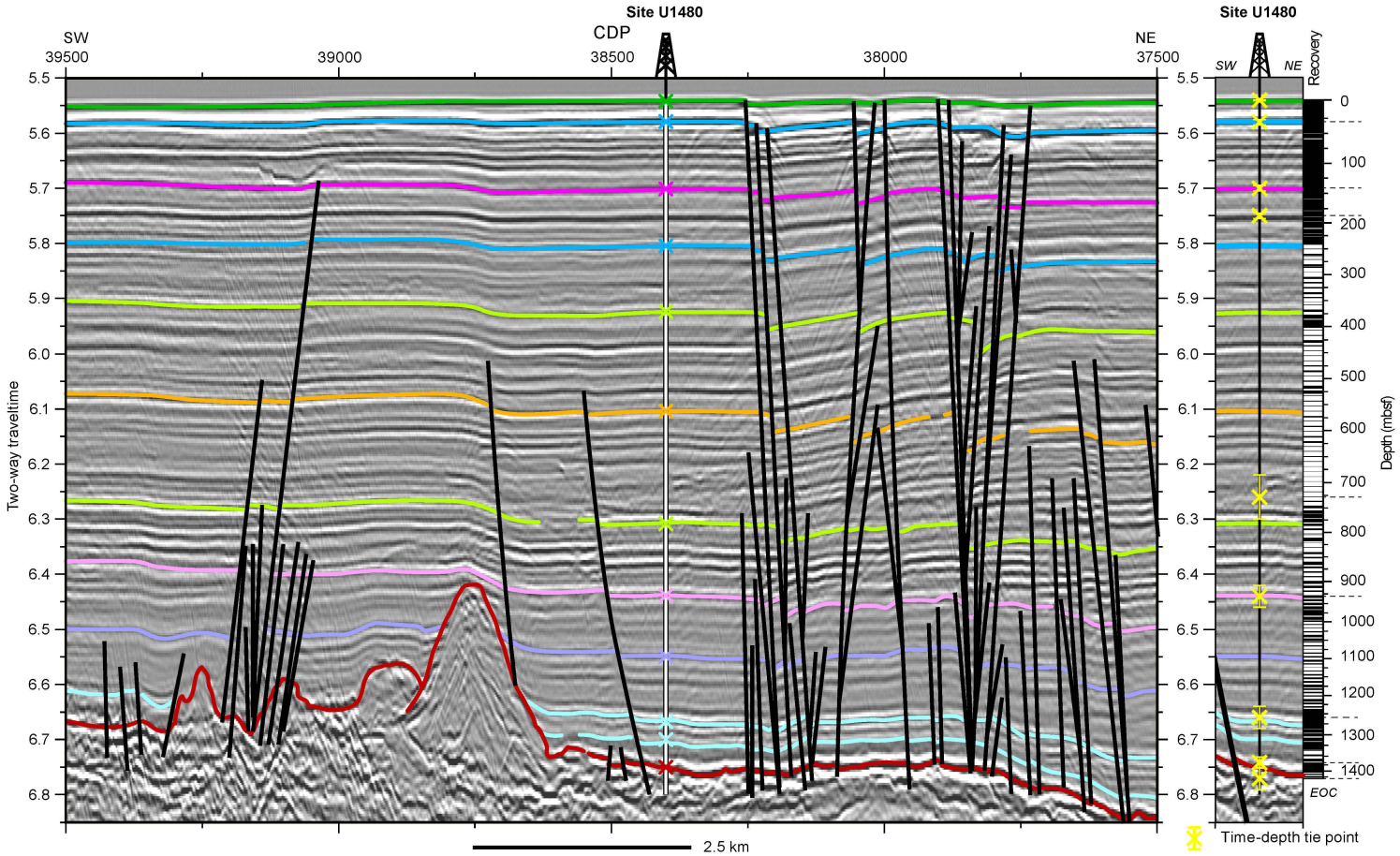
Site U1480
SW
CDP
NE
39500
39000
38500
38000
37500
Two-way traveltime
5.5
5.6
5.7
5.8
5.9
6.0
6.1
6.2
6.3
6.4
6.5
6.6
6.7
6.8
2.5 km
Site U1480
SW
NE
Recovery
0
100
200
300
400
500
600
700
800
900
1000
1100
1200
1300
1400
Depth (mbsf)
EOC
Time-depth tie point

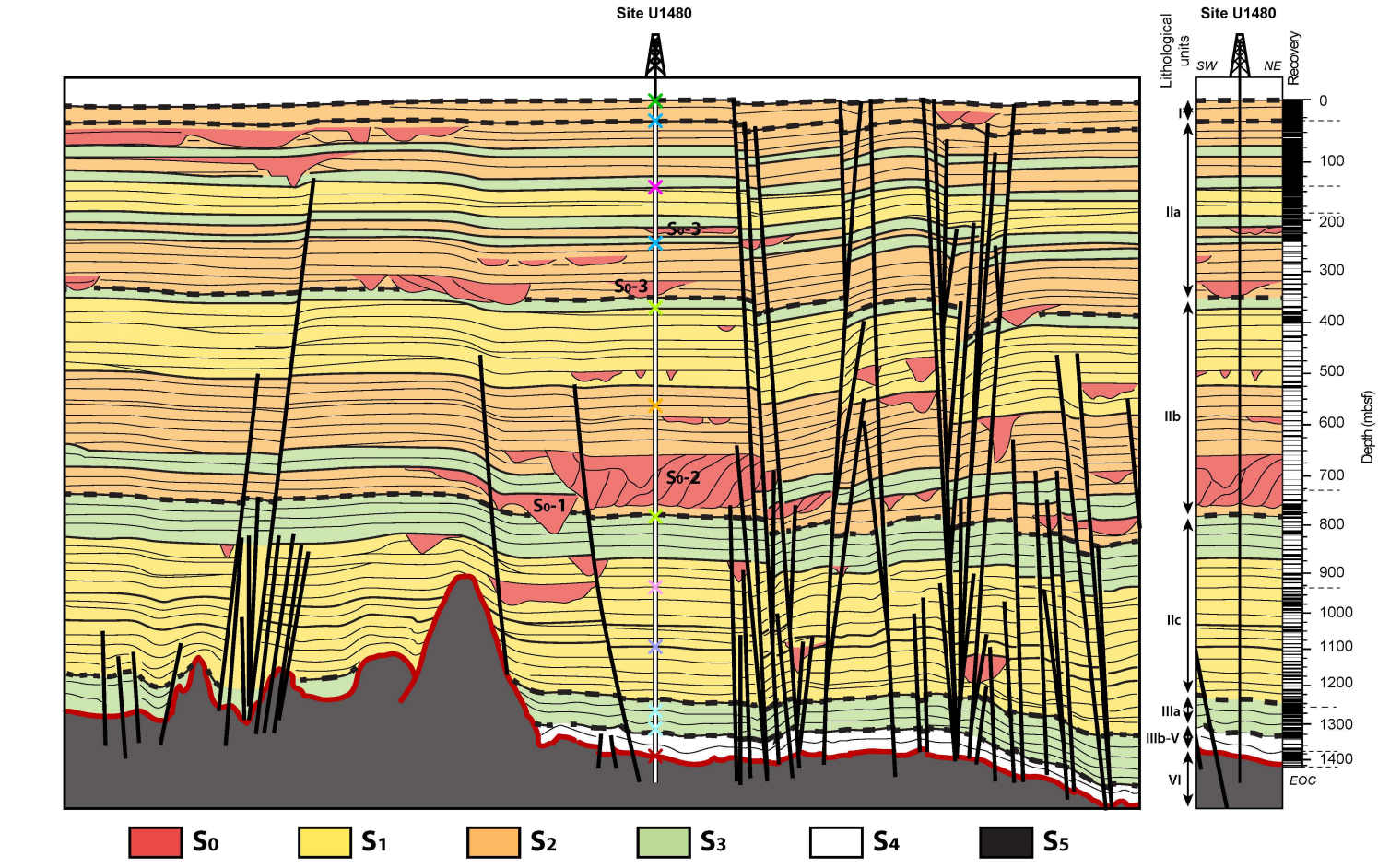
Site U1480
Site U1480
Lithological units
SW
NE
Recovery
I
IIa
IIb
IIc
IIIa
IIIb-V
VI
0
100
200
300
400
500
600
700
800
900
1000
1100
1200
1300
1400
Depth (mbsf)
EOC
S0-3
S0-3
S0-2
S0-1
S0
S1
S2
S3
S4
S5

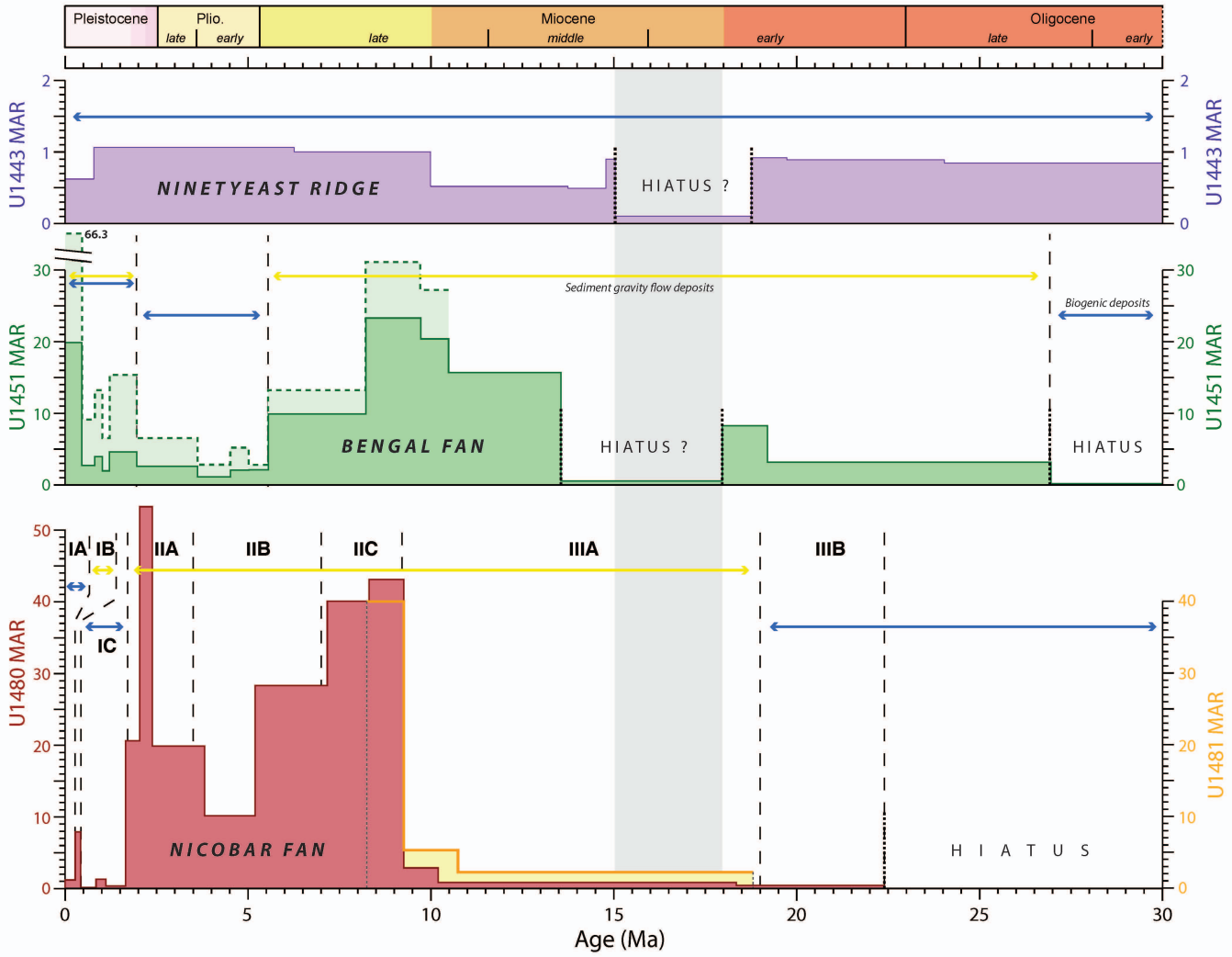
Pleistocene
Plio.
late
early
Miocene
late
middle
early
Oligocene
late
early
U1443 MAR
NINETYEAST RIDGE
HIATUS ?
66.3
Sediment gravity flow deposits
Biogenic deposits
U1451 MAR
BENGAL FAN
HIATUS ?
HIATUS
IA
IB
IC
IIA
IIB
IIC
IIIA
IIIB
U1480 MAR
U1481 MAR
NICOBAR FAN
H I A T U S
Age (Ma)

U1481G-61R-6

1325.54 - 1326.27 mbsf

22.4 Ma

U1481G-61R-7

1326.27 - 1327.02 mbsf

Hard Ground Surface
(Eocene-Oligocene hiatus ?)

core fracture

58.1±0.9 Ma

U1481G-61R-CC

1327.02 - 1327.18 mbsf

58.1±0.9 Ma

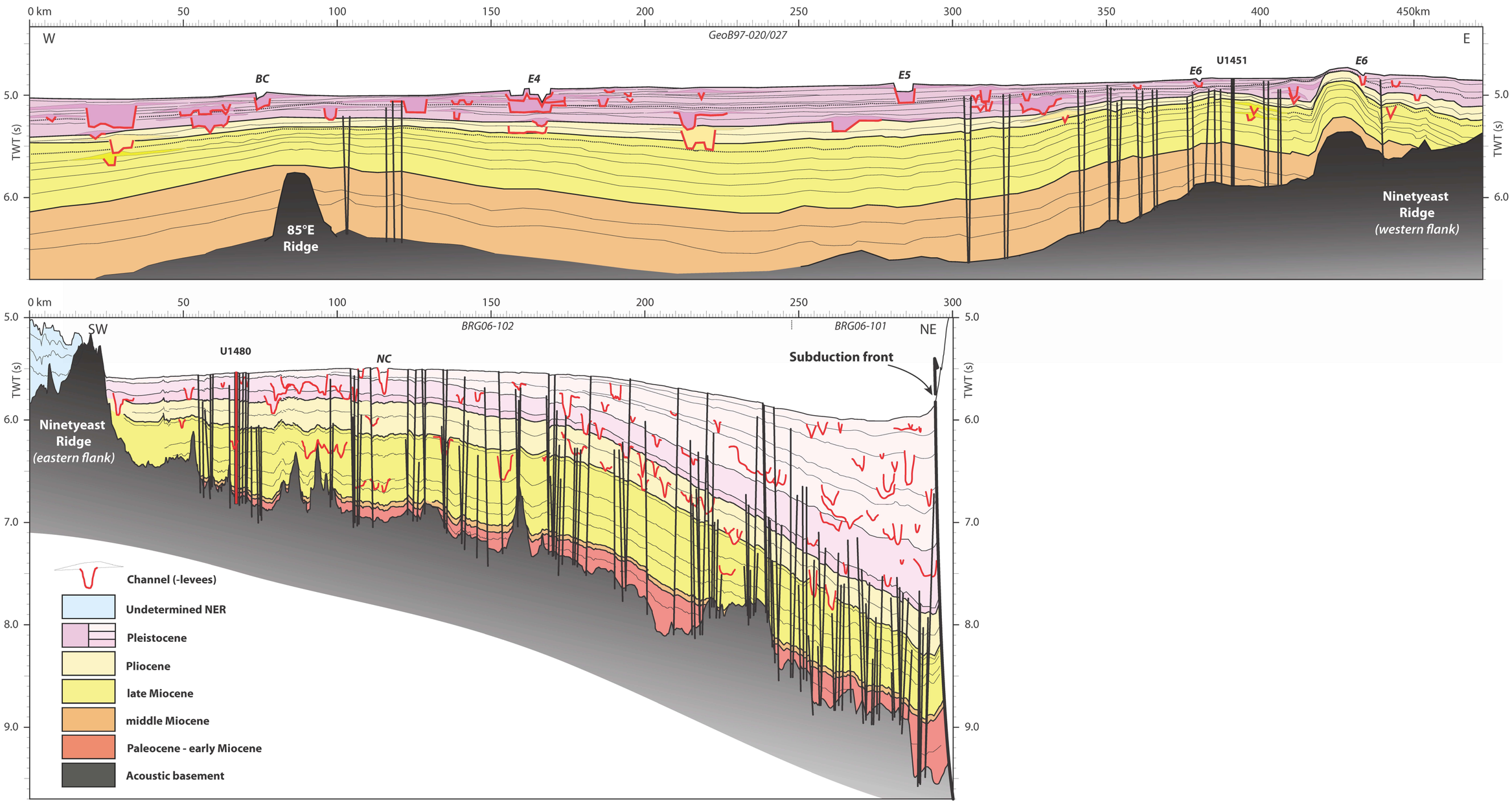
0 km
50
100
150
200
250
300
350
400
450km
W
E
GeoB97-020/027
BC
E4
E5
E6
U1451
E6
85°E
Ridge
Ninetyeast
Ridge
(western flank)
TWT (s)
5.0
6.0
SW
NE
BRG06-102
BRG06-101
U1480
NC
Subduction front
Ninetyeast
Ridge
(eastern flank)
7.0
8.0
9.0
Channel (-levees)
Undetermined NER
Pleistocene
Pliocene
late Miocene
middle Miocene
Paleocene - early Miocene
Acoustic basement

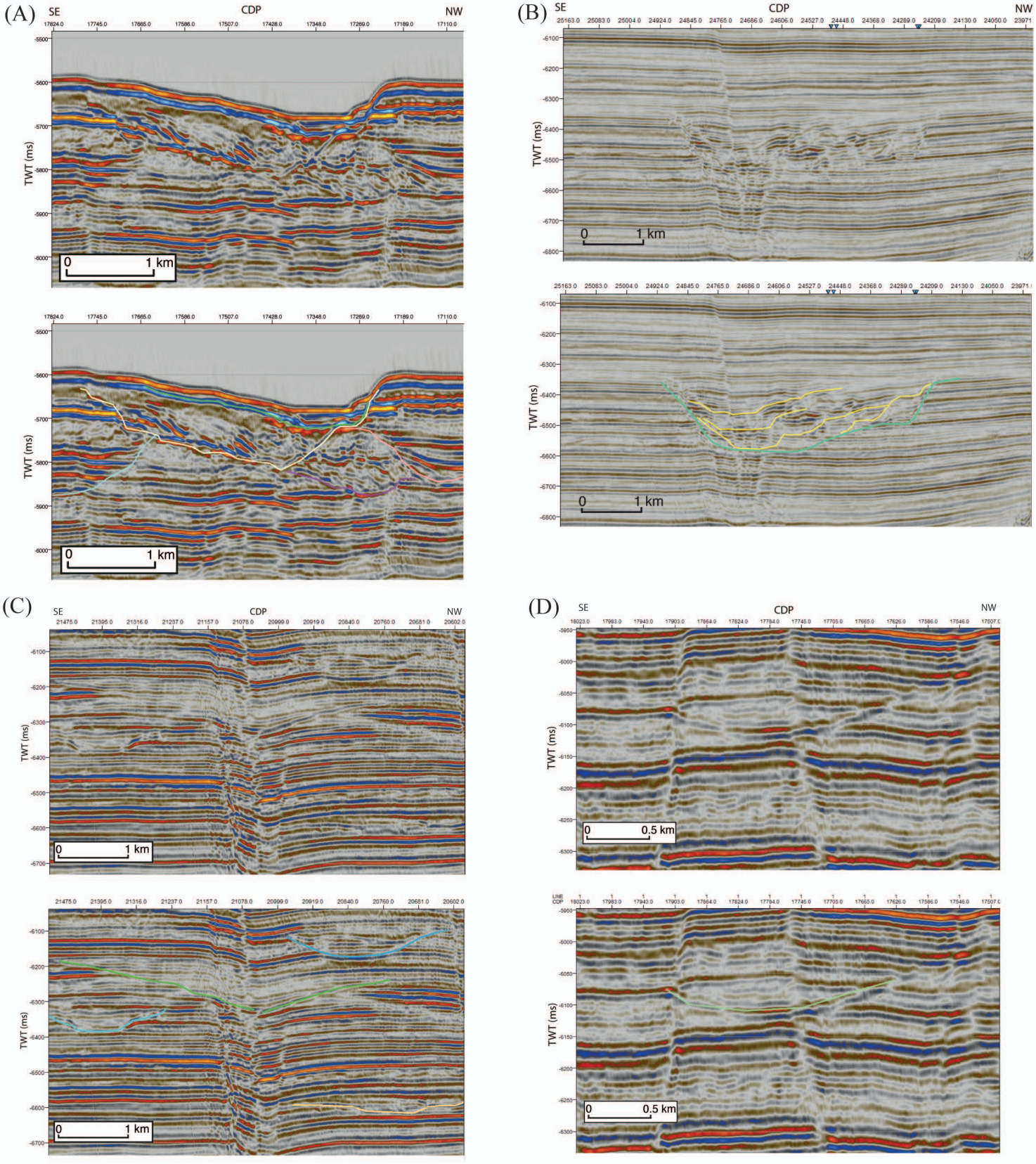
(A)
SE
CDP
NW
TWT (ms)
0
1 km
(B)
SE
CDP
NW
TWT (ms)
0
1 km
(C)
SE
CDP
NW
TWT (ms)
0
1 km
(D)
SE
CDP
NW
TWT (ms)
0
0.5 km

Figure 12.

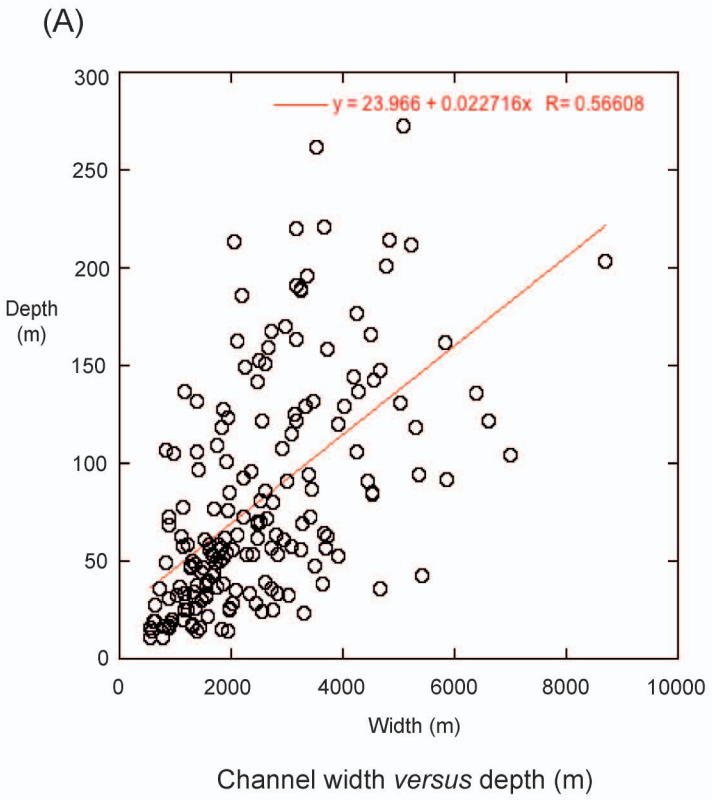

Channel width *versus* depth (m)

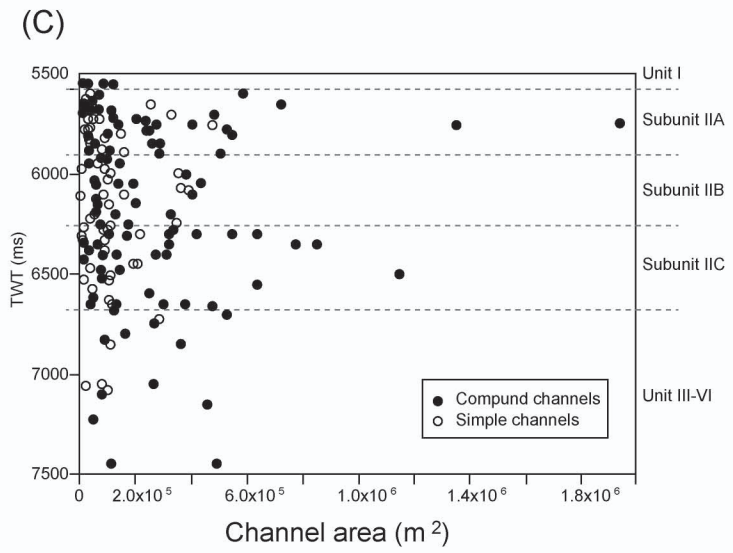

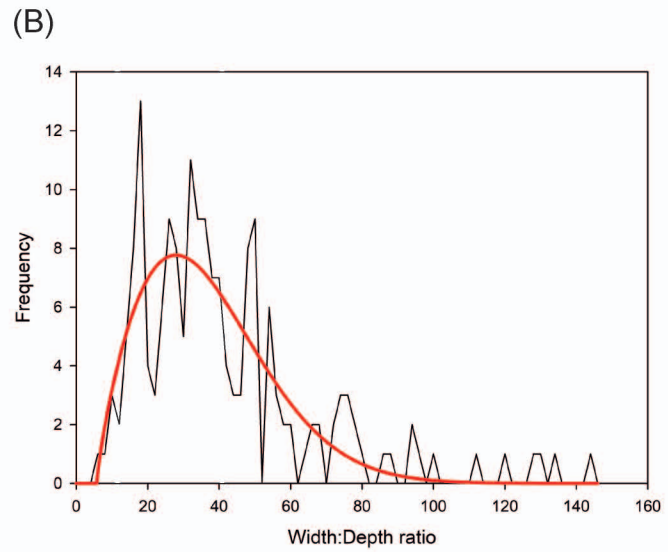

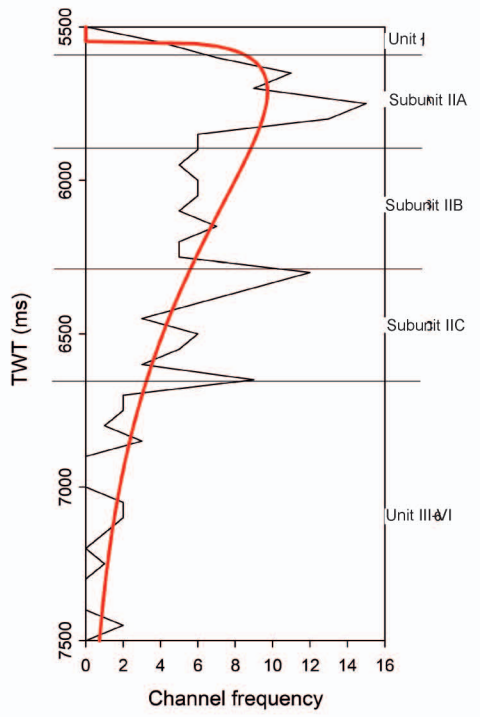

Figure 13

30 Ma

25 Ma

20 Ma

15 Ma

10 Ma

5 Ma

0 Ma

Legend

Depositional environments

- Land (Indian / Asian Plate)
- Shallow marine (Indian / Asian Plate)
- Abyssal (mainly pelagites)
- Submarine topographic high: seamount, ridge or plateau (mainly pelagites)
- Submarine fan (low SARs)
- Submarine fan (high SARs)

DSDP/ODP/IODP sites

- Older expeditions
- IODP 362

SGF pathways

- Principal source
- Primary pathways
- Secondary pathways